LIFE SCIENCES

The transmembrane endoplasmic reticulum–associated E3 ubiquitin ligase TRIM13 restrains the pathogenic-DNA–triggered inflammatory response

Xuelian Li[1,2]†, Zhou Yu[3,4]†, Qian Fang[2]†, Mingjin Yang[2]†, Jiaying Huang[1], Zheng Li[2], Jianli Wang[1,5,6]*, Taoyong Chen[2]*

The endoplasmic reticulum (ER)–localized stimulator of interferon genes (STING) is the core adaptor for the pathogenic-DNA–triggered innate response. Aberrant activation of STING causes autoinflammatory and autoimmune diseases, raising the concern about how STING is finely tuned during innate response to pathogenic DNAs. Here, we report that the transmembrane domain (TM)–containing ER-localized E3 ubiquitin ligase TRIM13 (tripartite motif containing 13) is required for restraining inflammatory response to pathogenic DNAs. TRIM13 deficiency enhances pathogenic-DNA–triggered inflammatory cytokine production, inhibits DNA virus replication, and causes age-related autoinflammation. Mechanistically, TRIM13 interacts with STING via the TM and catalyzes Lys^6-linked polyubiquitination of STING, leading to decelerated ER exit and accelerated ER-initiated degradation of STING. STING deficiency reverses the enhanced innate anti-DNA virus response in TRIM13 knockout mice. Our study delineates a potential strategy for controlling the homeostasis of STING by transmembrane ER-associated TRIM13 during the pathogenic-DNA–triggered inflammatory response.

INTRODUCTION

Innate immunity is the first and most rapid line of host defense against invading pathogens. Host cells initiate the innate immune response upon recognition of conserved pathogen-associated molecular patterns and host damage-associated molecular patterns by diverse pattern recognition receptors (PRRs), such as the Toll-like receptors (TLRs); the nucleotide binding and oligomerization, leucine-rich proteins (NLRs); the retinoic acid-inducible gene I (RIG-I)–like receptors; the absent in melanoma 2–like receptors; and the DNA receptors (*1*). Despite their critical roles in host antimicrobial responses, aberrant activation of PRR signaling pathways has been linked to autoinflammatory and autoimmune diseases (*1*).

Pathogenic DNAs derived from pathogens (such as genomic DNA of bacteria, DNA viruses, parasites, and DNA produced by retroviruses during the life cycle) and self-origin (such as DNA released from mitochondria and nuclei into cytosol and extracellular DNA contained in vesicles and taken by host cells) are potent immunostimulators of the DNA sensors (*2*–*5*). The cyclic guanosine monophosphate–adenosine monophosphate (cGAMP) synthase (cGAS), together with other DNA sensors [such as interferon (IFN) gamma inducible protein 16 (IFI16), DEAD-box helicase 41 (DDX41), Z-DNA binding protein 1 (ZBP1), and heterogeneous nuclear ribonucleoprotein A2/B1 (HNRNPA2B1)], is responsible for the recognition of pathogenic DNAs (*1*–*6*). These DNA sensors initiate signaling pathways that converge at the core adaptor STING [stimulator of IFN genes; also mediator of IFN regulatory factor 3 (IRF3) activation (MITA), endoplasmic reticulum (ER) IFN stimulator (ERIS), methionine-proline-tyrosine-serine amino acid sequence containing protein (MPYS), or transmembrane protein 173 (TMEM173)] (*7*–*11*). STING is a transmembrane ER-localized protein that plays indispensable roles in einnate anti-DNA virus response (*7*, *8*). In response to bacterial cyclic dinucleotides (CDNs) or cGAS-catalyzed cGAMP, STING exits the ER and then translocates to the Golgi apparatus through the ER-Golgi intermediate compartment (ERGIC), where STING recruits TBK1 [tumor necrosis factor receptor-associated factor (TRAF) family member associated nuclear factor κB (NF-κB) activator (TANK)-binding kinase 1] and activates IRF3 -and NF-κB–transcriptional factors, leading to the production of inflammatory cytokines and the expression of IFN-stimulated genes (ISGs) (*2*–*5*). STING has also been implicated in cell death, tumorigenesis, and antitumor immunity (*3*–*5*). Autosomal dominant gain-of-function mutations in human STING cause a severe autoinflammatory syndrome called STING-associated vasculopathy with onset in infancy (SAVI) (*12*, *13*). Various studies in human and mouse models have illustrated an extensive linkage of STING to multiple inflammatory or autoimmune disorders (*4*, *5*). These studies raise a key concern about the mechanism(s) for fine-tuning of STING activation and signaling, especially the negative regulators for STING.

Several mechanisms have been identified for the negative regulation of STING (*2*–*5*). The NLR proteins NLRX1 and NLRC3 as well as the ER-localized Ca^{2+} sensor STIM1 (stromal interaction molecule 1) inhibit STING activation through interaction with STING (*14*–*16*). Posttranslational modifications of STING protein can also negatively regulate STING activation and signaling. The kinase ULK1 [uncoordinated phenotype gene 51 (unc-51)-like kinase 1; also ATG1 (autophagy-related 1)] and the phosphatases PPM1A (protein phosphatase, Mg^{2+}/Mn^{2+} dependent 1A) and PTPN1/2 (protein tyrosine phosphatase non-receptor type 1 and 2) inhibit STING activation through modulating STING phosphorylation (*17*–*19*). The E3 ubiquitin ligases ring finger protein

[1]Institute of Immunology, Zhejiang University School of Medicine, Hangzhou 310058, China. [2]National Key Laboratory of Medical Immunology and Institute of Immunology, Second Military Medical University, Shanghai 200433, China. [3]Institute of Systems Medicine, Chinese Academy of Medical Sciences and Peking Union Medical College, Beijing 100005, China. [4]Suzhou Institute of Systems Medicine, Suzhou 215123, China. [5]Institute of Immunology, Bone Marrow Transplantation Centre of the First Affiliated Hospital, Zhejiang University School of Medicine, Hangzhou 310058, China. [6]Institute of Haematology, Zhejiang University and Zhejiang Engineering Laboratory for Stem Cell and Immunotherapy, Hangzhou 310058, China. *Corresponding author. Email: jlwang@zju.edu.cn (J.W.); chenty@immunol.org (T.C.) †These authors contributed equally to this work.

(RNF) 5 (RNF5), tripartite motif containing 29 (TRIM29), and TRIM30a promote STING degradation, while the deubiquitinases ubiquitin specific peptidase (USP) 13 (USP13) and USP21 impair the formation of STING signalosome (*20*–*25*). For ubiquitinated STING, the ubiquitin-binding selective autophagy receptor p62 (also SQSTM1) directs STING degradation through autophagic pathway (*26*). In addition, the metabolite nitro fatty acids inhibit STING activation by impairing STING palmitoylation (*27*). Among these studies, modulation of STING ubiquitylation by E3 ubiquitin ligases or deubiquitinases represents a kind of key negative mechanism, whereas several E3 ubiquitin ligases, such as autocrine motility factor receptor (AMFR), TRIM32, TRIM56, RNF26, and RNF218, have been implicated in ubiquitinating STING and facilitating STING activation (*28*–*32*). So, it is important to identify previously unknown E3 ubiquitin ligases with a previously unknown type of ubiquitination for appropriate and accurate control of STING stability and activation.

Most of the TRIM family proteins have been defined as E3 ubiquitin ligases, characterized by an N-terminal RING finger domain, one or two zinc finger domains (named B1 and/or B2 boxes), one coiled-coil region, and diverse C-terminal domains (*33*). TRIM13 [also ret finger protein 2 (RFP2)] is a unique transmembrane ER-localized E3 that has been implicated in ER stress, ER-associated degradation (ERAD), and autophagy (*34*–*38*). In the field of innate inflammatory response, TRIM13 inhibits tumor necrosis factor (TNF)–induced NF-κB activation and innate anti-RNA virus response but potentiates TLR2-initiated innate response (*39*–*41*). Here, we provide genetic and in vivo evidence for the negative role of TRIM13 in the pathogenic-DNA–triggered inflammatory response. TRIM13 deficiency causes autoinflammation in aged mice. Our study provides fresh mechanistic insights into controlling of STING homeostasis and illustrates TRIM13 as a negative regulator of STING-associated inflammation.

RESULTS

TRIM13 restrains DNA-triggered inflammatory responses

We have previously initiated a screen for key E3 ubiquitin ligases involved in immune response [Gene Expression Omnibus (GEO), accession number GSE72077] (*42*). In RAW264.7 macrophages before and after vesicular stomatitis virus and herpes simplex virus 1 (HSV-1) infection, the mRNA of *Trim13* was abundantly expressed. In the gene database BioGPS, human *Trim13* mRNA was highly expressed in testis and colon tissues as well as in blood cells, whereas mouse *Trim13* mRNA was widely expressed in many tissues and cells (especially high in macrophages). In the GEO databases for *Trim13* mRNA expression profile, *Trim13* mRNA was substantially up-regulated or down-regulated after infection with H1N1 influenza virus (GDS5409), tubercle bacillus (GDS4256 and GDS5819), *Listeria monocytogenes* (GDS5605), *Chlamydia pneumoniae* (GDS2651), or Gram-positive bacteria (GDS5819) under conditions such as ultraviolet radiation (GDS400), ionizing radiation (GDS1544), or heat stress (GDS3004) or during autoinflammatory diseases as allergy (GDS3082), systemic lupus erythematosus (SLE; GDS4889, GDS4990, and GDS4719), familial hypercholesterolemia and atherosclerosis (GDS3668), psoriasis (GDS4602), multiple sclerosis (MS; GDS4218 and GDS3920), or heart failure (GDS3115). These data suggest that *Trim13* may be involved in inflammatory and autoimmune responses.

When we were investigating the role of TRIM13 in the innate immune response, it was reported that TRIM13 was implicated in TNF- and TLR2-initiated responses and in innate anti-RNA virus responses (*39*–*41*). In this study, we focused on DNA-triggered innate responses. In mouse peritoneal macrophages (PMs) and bone marrow–derived macrophages (BMDMs), *Trim13* mRNA was up-regulated after HSV-1 infection, along with the induction of *Ifnb* and *Il6* mRNAs (fig. S1, A and B). We then silenced the expression of TRIM13 in PMs and human HeLa cells (fig. S1, C and D). Although all three small interfering RNAs (siRNAs) for mouse or human *Trim13* enhanced the induction of inflammatory cytokines by HSV-1, the #3 siRNA of *Trim13* could most efficiently promote cytokine induction by HSV-1 (fig. S1, E and F) and was thus used in further experiments. We found that TRIM13 knockdown enhanced the induction of IFNβ, TNF, and IL-6 (interleukin-6) after HSV-1 infection or after treatments with poly (dA:dT) [poly-deoxyadenine-deoxythymine nucleotides (pdAT)] and synthesized cGAMP in PMs (fig. S1, G to J). In human HeLa cells, knockdown of TRIM13 also enhanced the induction of inflammatory cytokines by HSV-1 infection and by transfection of poly (dA:dT) and cGAMP (fig. S1, K to M), whereas the induction of anti-inflammatory cytokines *Il10* and *Tgfb* was not significantly altered in *Trim13*-silenced or *Trim13*-depleted PMs after HSV-1 infection (fig. S1N). In RAW264.7 macrophages, TRIM13 overexpression reduced the induction of inflammatory cytokines (fig. S2, A to E). Therefore, TRIM13 can restrain both pathogenic-DNA– and cGAMP-triggered inflammatory responses.

Previously, the E3 ubiquitin ligases RNF5, TRIM29, and TRIM30a have been identified as a negative regulator of STING by promoting STING degradation (*20*–*23*). So, we compared the effects of *Trim13* knockdown on the pathogenic-DNA–triggered inflammatory response to that of *Rnf5*, *Trim29*, and *Trim30a* knockdown. In macrophages, the mRNA expression of *Trim13* was abundant, together with *Rnf5* and *Trim30a*, while *Trim29* was of low expression (fig. S3A). After knockdown of *Rnf5*, *Trim29*, and *Trim30a* in PMs (fig. S3B), we found that the induction of *Ifnb* and *Il6* by HSV-1 infection was significantly increased to different extent, resembling to the effects of *Trim13* knockdown (fig. S3C). These preliminary data provoked us to further investigate the roles of TRIM13 in the innate anti-DNA response.

TRIM13 deficiency exaggerates DNA-triggered inflammatory responses

To validate the role of TRIM13 in regulating innate response to pathogen-derived DNA, we established $Trim13^{-/-}$ mice by recombinantly deleting exon 3 of *Trim13* with insertion of LoxP sequence at both ends and breeding the mice with EIIA-Cre mice (complete knockout). In $Trim13^{-/-}$ PMs and BMDMs, we found that the levels of inflammatory cytokines induced by HSV-1 infection and by transfection of poly (dA:dT) and cGAMP were all significantly increased, as compared to $Trim13^{+/+}$ macrophages (Fig. 1, A to H). In $Trim13^{-/-}$ BMDMs, the production of IFNβ, TNF, and IL-6 could be rescued by the overexpression of wild-type (WT) TRIM13 but not by TRIM13 without E3 ligase activity [mutations of Cys^{10} and Cys^{13} in the ring domain into Ala (TRIM13-CA); Fig. 1, I and J], indicating that the enhanced inflammatory response in $Trim13^{-/-}$ BMDMs was because of TRIM13 deficiency and was probably dependent on the E3 ligase activity of TRIM13. These data suggest that TRIM13 is required for restraining the inflammatory response to pathogen DNAs.

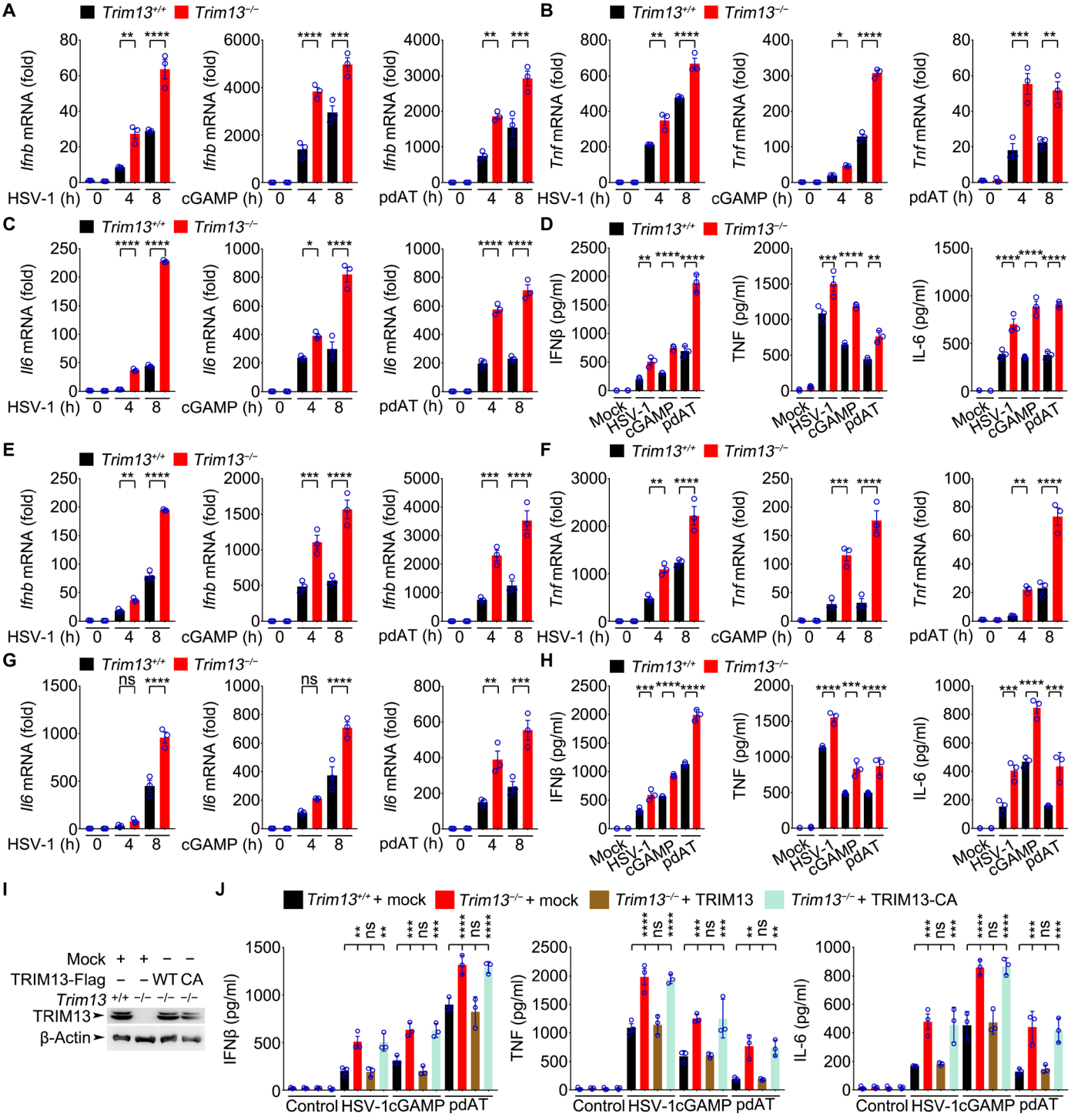

Fig. 1. TRIM13 deficiency amplifies the inflammatory response to DNA and cGAMP. (**A** to **H**) PMs (A to D) and BMDMs (E to H) were infected with HSV-1 [multiplicity of infection (MOI) = 5] or treated with cGAMP (5 μg/ml) or poly (dA:dT) (5 μg/ml) as indicated (A to C and E to G) or for 8 hours (D and H). mRNA levels of cytokines were examined by quantitative polymerase chain reaction (qPCR) (A to C and E to G), and cytokines in supernatants were measured by enzyme-linked immunosorbent assay (ELISA) (D and H). (**I** and **J**) *Trim13*$^{+/+}$ or *Trim13*$^{-/-}$ BMDMs were transfected with mock, TRIM13, or TRIM13-CA (CA) vectors for 48 hours. TRIM13 expression was examined by Western blotting (I). After infection with HSV-1 (MOI = 5) or treatment with cGAMP (5 μg/ml) or poly (dA:dT) (5 μg/ml) for 8 hours, cytokines in supernatants were measured by ELISA (J). Results are presented as means ± SE [A to H and J; one-way analysis of variance (ANOVA) followed by Bonferroni multiple comparison] of three independent experiments ($n = 3$; from three WT or KO mice). One representative experiment of three is shown. ns, not significant. *$P < 0.05$, **$P < 0.01$, ***$P < 0.001$, and ****$P < 0.0001$.

To confirm the enhanced responsiveness of *Trim13*$^{-/-}$ BMDMs to other pathogenic DNAs, we transfected genomic DNAs derived from autologous thymocytes and B16 melanoma cells after treatments with chemotherapeutic drugs (dexamethasone, mitomycin C, and cisplatin). We found that these autologous DNAs induced the production of inflammatory cytokines while TRIM13 deficiency significantly enhanced the response (fig. S4), suggesting that TRIM13 was a negative regulator of both autologous pathogenic-DNA–triggered responses, and pathogen-derived DNA-triggered inflammatory responses.

TRIM13 deficiency promotes innate anti-DNA virus response

We then tested whether TRIM13 plays an important role during innate response to DNA virus HSV-1. We intraperitoneally injected sublethal dosages of HSV-1 [2×10^8 plaque-forming units (PFUs) per mouse] into mice. We found that the amounts of IFNβ, TNF, and IL-6 contained in serum were significantly increased in *Trim13*$^{-/-}$ mice while the HSV-1 loads in the liver, spleen, and lung were significantly reduced (Fig. 2, A to E). Histological examination of the lung tissues 24 hours after HSV-1 infection showed that the infiltration of inflammatory cells in the lung of *Trim13*$^{-/-}$ mice was significantly enhanced (Fig. 2, F and G), which was further confirmed by counting of CD45$^+$ immune cells in bronchoalveolar lavage fluids (BALFs) (Fig. 2H). When HSV-1 viruses were intravenously injected, we found that the replication of HSV-1 in the brain was significantly reduced in *Trim13*$^{-/-}$ mice (Fig. 2, I and J). To evaluate the effects of TRIM13 loss on protection of host from DNA virus infection, we

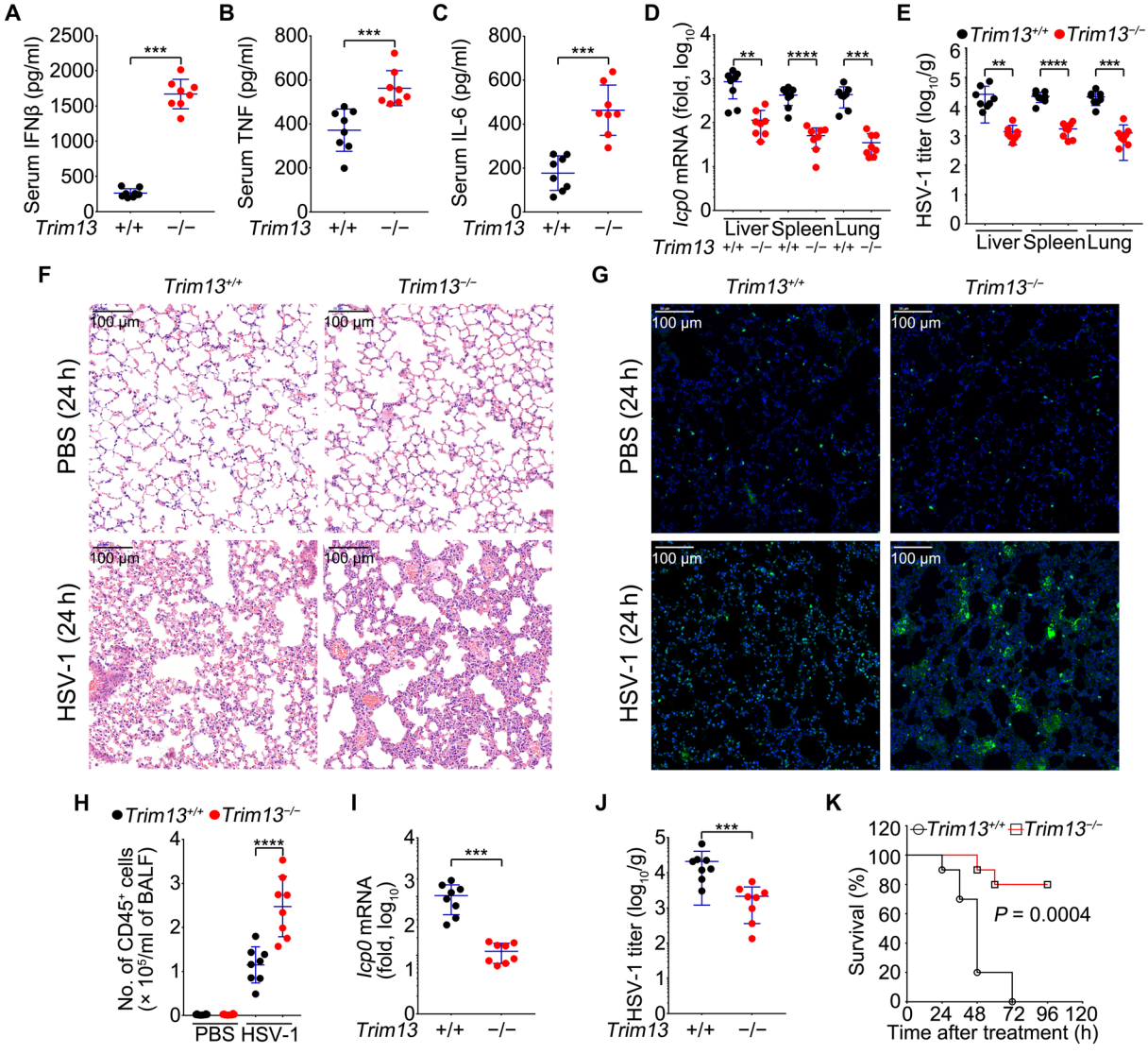

Fig. 2. TRIM13 deficiency promotes innate anti-DNA virus response in vivo. (**A** to **H**) *Trim13*$^{+/+}$ or *Trim13*$^{-/-}$ mice ($n = 8$ mice) were intraperitoneally injected with 100 μl of phosphate-buffered saline (PBS) or PBS containing 2×10^8 PFUs of HSV-1. Twelve hours later, serum levels of cytokines were measured by ELISA (A to C). Alternatively, 24 hours after pathogen infections, the HSV-1 titers in tissues ($n = 8$ mice) were determined (D and E). The lung tissues were examined by hematoxylin and eosin (H&E) staining (F) or by immunofluorescent microscope for CD45$^+$ immune cells (G). Cells derived from BALFs were stained for CD45$^+$ cells and counted by FACS (fluorescence-activated cell sorting) (H). (**I** and **J**) Mice ($n = 8$) were intravenously injected with 100 μl of PBS containing 2×10^8 PFUs of HSV-1. Seventy-two hours after treatments, the replication status of HSV-1 in the brain was evaluated. (**K**) Mice ($n = 10$) were intraperitoneally injected with 100 μl of PBS containing 5×10^8 PFUs of HSV-1. Results are presented as means ± SD (A to E and H to J; unpaired Student's *t* test). One representative experiment of three is shown. $^{**}P < 0.01$, $^{***}P < 0.001$, and $^{****}P < 0.0001$.

intraperitoneally injected lethal dosages of HSV-1 (5×10^8 PFUs per mouse) in mice. We found that the survival of *Trim13*$^{-/-}$ mice was significantly improved (Fig. 2K). These data suggest that TRIM13 is required for restraining the inflammatory response to and restricting the protection of host from DNA virus invasion.

TRIM13 deficiency potentiates DNA virus–triggered NF-κB and IRF3 activation

To investigate the signaling mechanisms of TRIM13 on innate anti-DNA virus response, we examined the activation of signaling mediators responsible for inducing inflammatory cytokines after infection with HSV-1 and VACV (vaccinia virus) in BMDMs. We found that TRIM13 deficiency enhanced the phosphorylation of TBK1, IRF3, IκBα (inhibitor of NF-κB α), and p65 (also RelA), but not ERK1/2 (extracellular signal–regulated kinase 1/2), JNK1/2 (c-Jun N-terminal kinase 1/2), and p38 (Fig. 3, A and B, and fig. S5, A and B). Meanwhile, we found that the nuclear translocation of p65 and IRF3 as well as the dimerization of IRF3 were enhanced in *Trim13*$^{-/-}$ BMDMs (Fig. 3, C to F, and fig. S5, C and D). These data suggest that TRIM13 deficiency facilitates DNA virus–triggered activation of TBK1-IRF3 and NF-κB pathways.

Because TRIM13 negatively regulated cGAMP-triggered cytokines, we examined the effects of TRIM13 on STING-directed activation of IRF3 and NF-κB by using luciferase reporters. We found that TRIM13 overexpression inhibited STING- and cGAMP-induced activation of *Ifnb* and NF-κB reporters (Fig. 3, G and H), whereas the TBK1- and IRF3-induced activation of *Ifnb* as well as the TBK1-, IKKβ (IκB kinase β)–, and p65–induced activation of NF-κB reporters were not affected (fig. S5, E to H). When STING was cotransfected with TRIM13 without transmembrane domain (TM; 1 to 315 amino acids of TRIM13, termed TRIM13-ΔTM) or TRIM13 without E3 activity (TRIM13-CA), we found that these two mutants could not inhibit cGAMP-induced activation of *Ifnb* and NF-κB reporters (Fig. 3I). These data indicate that TRIM13 inhibits the activation of TBK1-IRF3 and NF-κB pathways at the level of STING.

TRIM13 interacts with STING via the TM

To elucidate the molecular mechanisms involved in TRIM13-mediated regulation of innate response, we initially (without the awareness about the association of TRIM13 with STING) examined the partners of TRIM13 by using liquid chromatography (LC)–mass spectrometry in human embryonic kidney (HEK) 293T cells after overexpression and immunoprecipitation (IP) of TRIM13. We found that TRIM13 was associated with abundant ER-related proteins and other vesicular proteins (table S1). However, STING was not detected possibly because of the absence of STING in the HEK293T cell model used. In WT BMDMs, we found that endogenous TRIM13 could interact with STING at resting state, while this interaction was attenuated after HSV-1 infection (Fig. 4A). In STING-deficient RAW264.7 cells, we found that the overexpressed TRIM13 could not bind TBK1 and IRF3 anymore (Fig. 4B), indicating that TRIM13 may interact with TBK1 and IRF3 via STING.

Next, we examined the localization of TRIM13 in RAW264.7 cells. We found that TRIM13 was colocalized with ER proteins (staining for KDEL), but not with endosomal [staining for EEA1 (early endosome antigen 1)], mitochondrial [staining for TOM20 (translocase of outer membrane 20)], and Golgi apparatus (staining for Golgi 58K) proteins (Fig. 4C and fig. S6, A and B). In both RAW264.7 cells and HeLa cells, the bulk of TRIM13 remained in ER after HSV-1 infection (Fig. 4C). After activation by bacterial CDNs or cGAMP, STING exits the ER and transports through ERGIC to Golgi apparatus for activation or terminal degradation (*2*–*5*). In both RAW264.7 cells and in HeLa cells, TRIM13 was colocalized with STING under resting state (Fig. 4, D and E). After HSV-1 infection, the colocalization of TRIM13 with STING was attenuated (Fig. 4, D and E, and fig. S4C), which was consistent with what was observed in IP assays (Fig. 4A). Therefore, TRIM13 colocalizes with STING at the ER membrane, while DNA virus infection does not radically change TRIM13 localization.

STING contains four TM segments (TMs 1 to 4) in its N terminus, and its C terminus contains a dimerization domain, a CDN binding region (CBD), and a C-terminal tail (CTT) (*2*–*5*), whereas TRIM13 contains three conserved domains—RING (R), B-Box (B), and coiled-coil (CC)—in its N terminus and a TM in its C terminus (Fig. 4F) (*33*). We determined which domain(s) in STING and TRIM13 were responsible for the interaction. Full-length TRIM13 could bind full-length (FL) STING or the TM of STING (#1), but not STING without TM (#2) (Fig. 4G). Meanwhile, the full-length STING could bind full-length TRIM13 or TRIM13 without RING domain (#1), but not TRIM13 without TM (#2) or TRIM13 with only RING domain (#3) (Fig. 4H). TRIM13 and STING without TM could not be colocalized when examined by confocal microscopy (fig. S6B). These data suggest that TRIM13 and STING interact with each other through their TMs.

TRIM13 catalyzes Lys^6 linkage of STING on Lys^{19}

Because TRIM13 is an E3 ubiquitin ligase, we investigated the effects of TRIM13 on STING ubiquitylation to resolve the underlying molecular mechanisms for TRIM13-elicited inhibition of STING signaling. In both *Trim13*$^{+/+}$ and *Trim13*$^{-/-}$ BMDMs, the Lys^{48}- and Lys^{63}-linked polyubiquitinations of STING were not affected after DNA virus infections (HSV-1 and VACV) (Fig. 5, A and B). However, the overall polyubiquitination of STING was reduced in *Trim13*$^{-/-}$ BMDMs after DNA virus infections (Fig. 5C). Moreover, in HEK293T cells, overexpression of TRIM13 enhanced the polyubiquitination of exogenously expressed STING, while TRIM13 without the E3 ligase activity (TRIM13-CA) failed to polyubiquitinate STING (Fig. 5D), indicating that TRIM13 catalyzed STING polyubiquitination relying on its E3 ligase activity.

After overexpression of TRIM13, STING, and WT or mutated ubiquitin (Ub; with the only indicated Lys residue unchanged; fig. S7A) in HEK293T cells, we found that STING was linked to a Lys^6-only ubiquitin mutant (Ub #1; Fig. 5E), indicating that TRIM13 catalyzed Lys^6 linkage of STING. To identify the Lys residue in STING modified by TRIM13, we mutated all the 12 Lys residues into Arg in mouse STING one by one (fig. S7B). In HEK293T cells, we found that the Lys^{19} residue at the N terminus of STING (before the first TM of STING) was the ubiquitin linkage site for TRIM13 because mutation of this residue into Arg (STING-K19R, #1) failed to be polyubiquitinated by TRIM13 (Fig. 5F).

To confirm the significance of Lys^{19} in STING in DNA-triggered innate responses, we reexpressed STING and the STING-K19R mutant in *Sting*$^{-/-}$ RAW264.7 cells (fig. S8A). We found that WT STING could rescue the IFNβ and IL-6 production in *Sting*$^{-/-}$ RAW264.7 cells induced by HSV-1 infection while STING-K19R increased the cytokine production (fig. S8, B and C), which may be because of the durative STING levels in STING-K19R–rescued *Sting*$^{-/-}$ RAW264.7 cells after HSV-1 infection (fig. S8, D and E). Moreover,

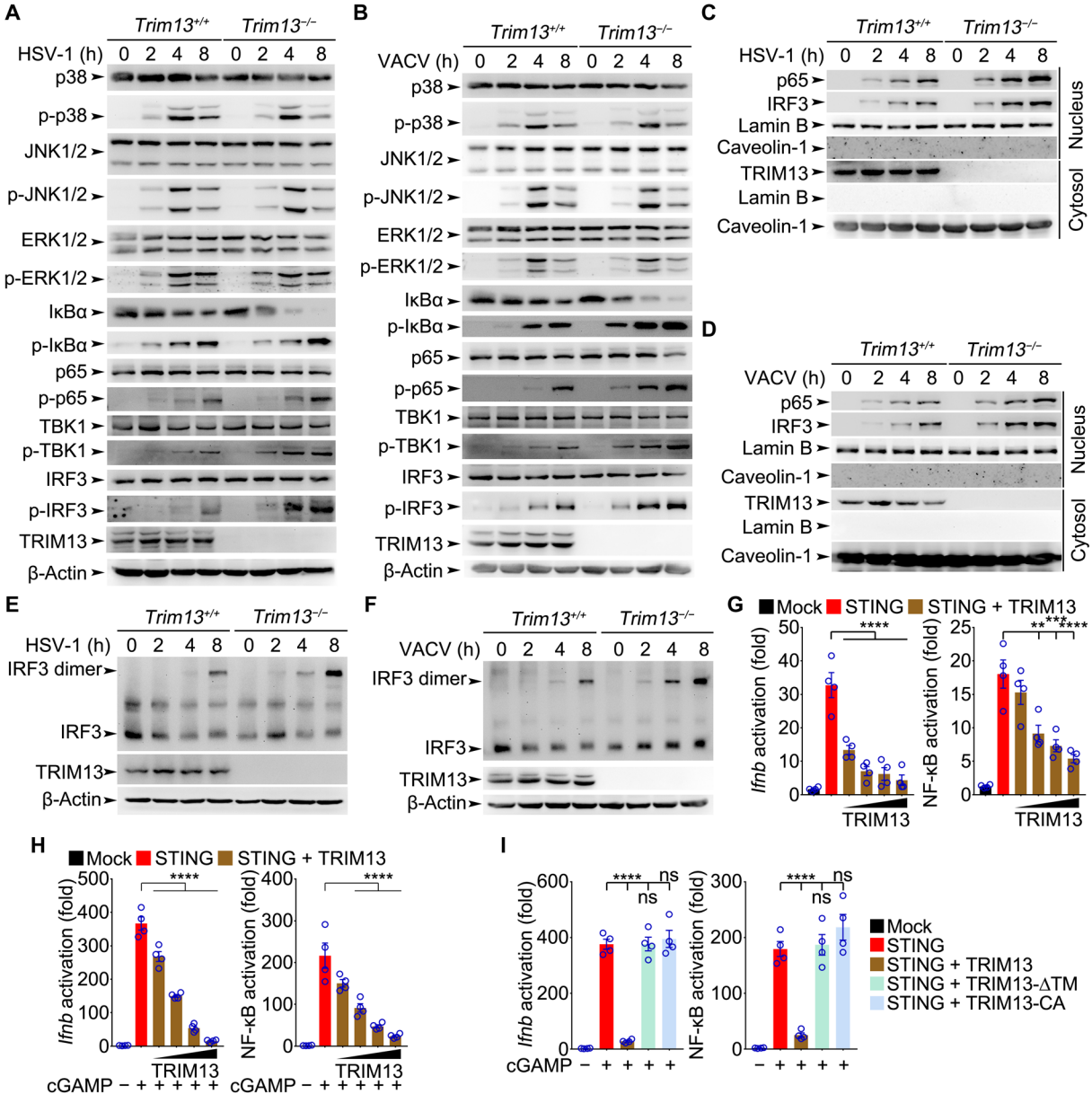

Fig. 3. TRIM13 is required for restraining the activation of both TBK1-IRF3 and NF-κB signaling pathways. (**A** to **F**) *Trim13*$^{+/+}$ or *Trim13*$^{-/-}$ BMDMs were infected with HSV-1 (MOI = 5) or VACV (MOI = 5) as indicated. Whole-cell extracts (WCE) (A and B) as well as nuclear and cytosolic extracts (C and D) were examined for signaling mediators by Western blotting. Otherwise, nondenatured lysates were separated in native polyacrylamide gel electrophoresis (PAGE) gel and then examined by Western blotting for IRF3 (E and F). (**G** to **I**) Human embryonic kidney (HEK) 293T cells were transfected with mock, STING, Flag-tagged TRIM13 (100, 200, 300, or 400 ng), or TRIM13 mutants (TRIM13-ΔTM or TRIM13-CA) vectors and indicated reporter vectors. Forty-eight hours later, the cells were treated with or without cGAMP (5 μg/ml) for 8 hours, and the luciferase activity was determined ($n = 4$ biological samples per group). Results (G to I) are presented as means ± SD (one-way ANOVA followed by Bonferroni multiple comparison). One representative experiment of three is shown. $^{**}P < 0.01$, $^{***}P < 0.001$, and $^{****}P < 0.0001$.

we found that the STING-K19R–rescued *Sting*$^{-/-}$ RAW264.7 cells showed increased IFNβ and IL-6 production even in case when TRIM13 was overexpressed (fig. S8, F to H). These data suggest that TRIM13 polyubiquitinates STING on Lys[19], which serves as a negative mechanism for regulating innate response to DNA virus.

TRIM13 deficiency accelerates removal of STING from ER

The above data have shown that TRIM13 interacts with and polyubiquitinates STING. According to the current models for STING activation and termination, STING dimerizes upon CDN binding and then exits ER to Golgi apparatus and to post-Golgi vesicles for STING signalosome assembly or for autophagosomal and autophagic degradation (*2*–*5*, *43*–*45*). Considering that TRIM13 colocalizes with STING in ER and acts as an E3 ligase for STING, we hypothesize that TRIM13 may affect the dimerization of STING, ER exit of STING, and degradation of STING.

We examined the STING dimerization after HSV-1 or VACV infections. We found that TRIM13 deficiency enhanced the dimerization

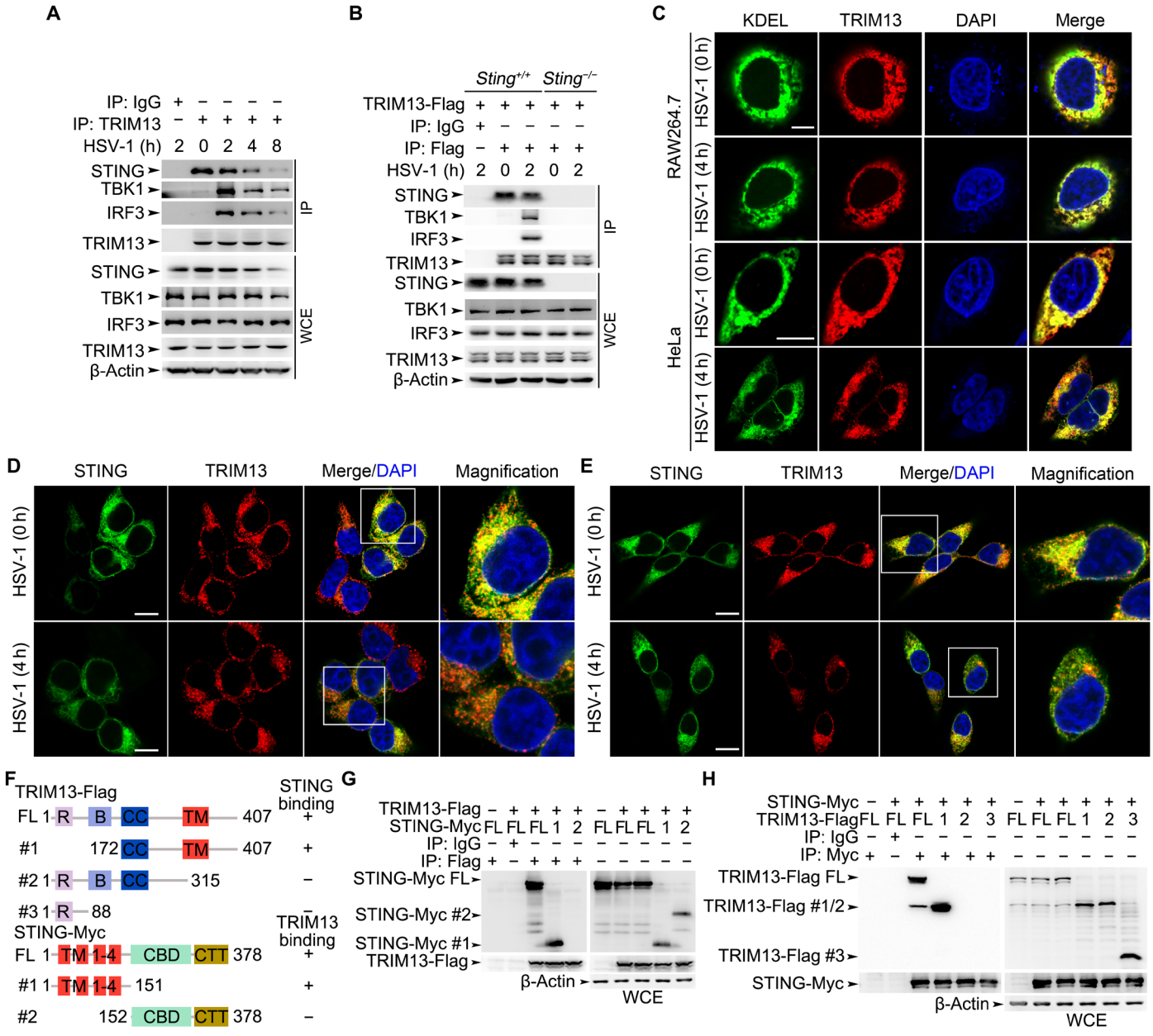

Fig. 4. TRIM13 interacts with STING via their TMs. (**A** and **B**) WT BMDMs (A) or *Sting*$^{-/-}$ RAW264.7 cells (B) were infected with HSV-1 (MOI = 5) as indicated. After IP with anti-TRIM13 antibody (A) or anti-Flag antibody (B), components in the complex were examined by Western blotting. (**C** to **E**) RAW264.7 cells (C and D) or HeLa cells (C and E) were transiently transfected with green fluorescent protein (GFP)–tagged STING or red fluorescent protein (RFP)–tagged TRIM13 for 36 hours, and then infected with or without HSV-1. Cells were then examined by confocal microscope (C to E). Scale bars, 10 μm. (**F**) Schematic diagram of domains in full-length (FL) or fragments of TRIM13-Flag or STING-Myc. Numerical numbers indicate for the site of amino acids. (**G** and **H**) HEK293T cells were transiently transfected with Flag-tagged TRIM13 (or mutants) and Myc-tagged STING (or mutants) as indicated for 48 hours. WCE were immunoprecipitated with anti-Flag Sepharose beads (G) or anti-Myc Sepharose beads (H), and the associated STING or TRIM13 proteins were examined by Western blotting. One representative experiment of three is shown.

of STING in BMDMs (Fig. 6, A and B). To investigate the effects of TRIM13 on the ER exit of STING, we isolated ER fractions from *Trim13*$^{+/+}$ and *Trim13*$^{-/-}$ BMDMs and examined the amounts of STING in ER after DNA virus infection. We found that HSV-1 or VACV infection triggered the removal of STING from ER while TRIM13 deficiency accelerated this process (Fig. 6, C and D, and fig. S9, A and B), indicating that TRIM13 may delay the removal of STING from ER. In *Trim13*$^{-/-}$ mouse embryonic fibroblast (MEF) cells, we also observed the accelerated removal of STING from ER after HSV-1 infection (Fig. 6E and fig. S9C).

To distinguish that the accelerated removal of STING from ER of *Trim13*$^{-/-}$ BMDMs was not because of the overall STING degradation, we examined the ER-associated STING in BMDMs in the presence of proteasome inhibitor MG132, which had been demonstrated to reverse several E3 ligase–elicited STING degradation (*20*–*23*). We found that *Trim13*$^{-/-}$ BMDMs still demonstrated accelerated

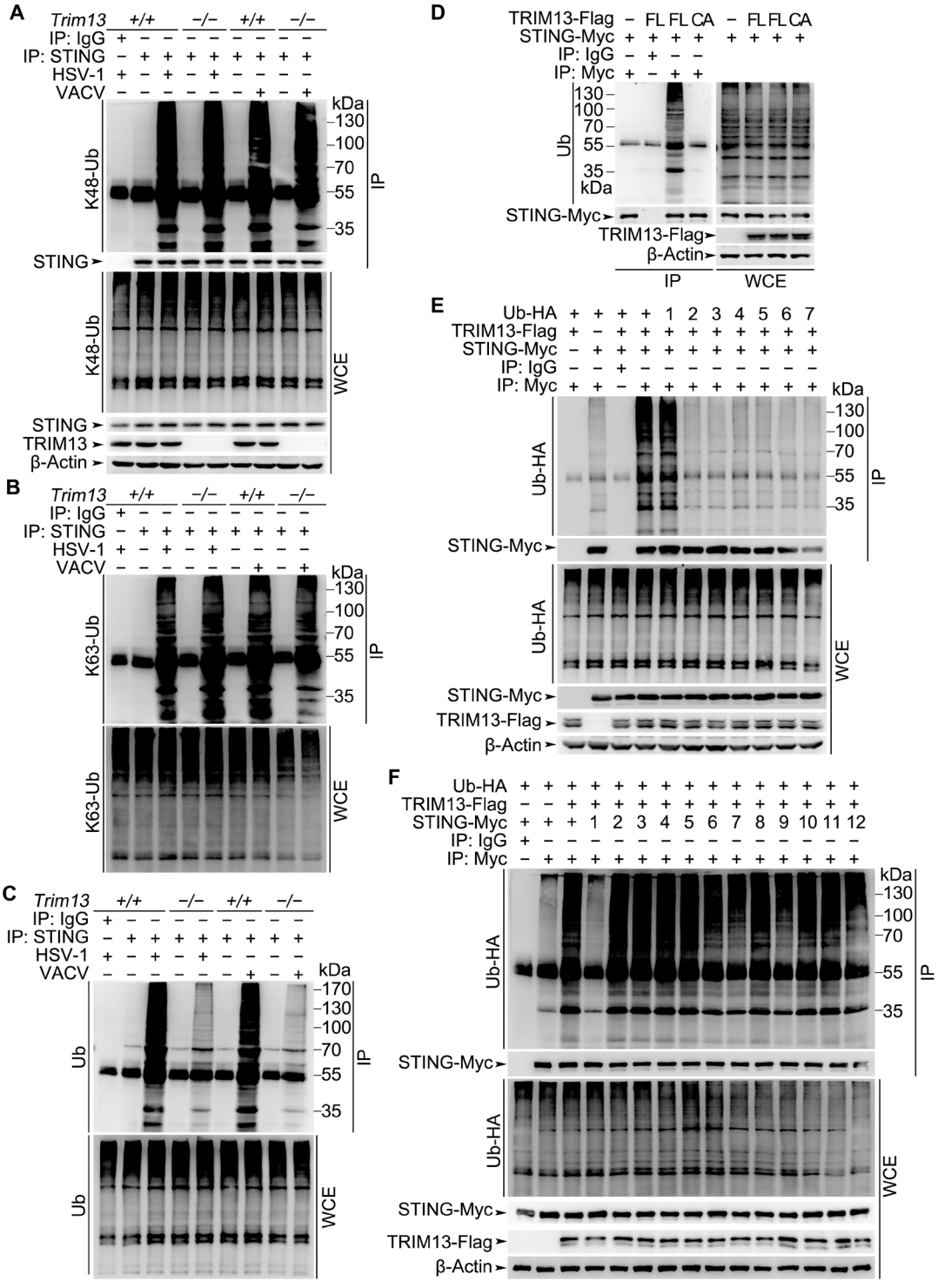

Fig. 5. TRIM13 catalyzes Lys^{6}-linked polyubiquitination of STING on Lys^{19}. (**A** to **C**) *Trim13*$^{+/+}$ or *Trim13*$^{-/-}$ BMDMs cells were infected with HSV-1 (MOI = 5) or VACV (MOI = 5) for 4 hours. Then, WCE were immunoprecipitated with anti-STING antibody plus protein A/G beads. Polyubiquitination of STING was examined by Western blotting using anti-K48 ubiquitin (Ub) (**A**), anti-K63 Ub (**B**), or anti-Ub (**C**) antibodies. (**D**) HEK293T cells were transiently transfected with Flag-tagged TRIM13 (FL) or TRIM13-CA (CA) together with Myc-tagged STING vectors as indicated for 48 hours. Then, polyubiquitination of STING was examined by Western blotting after IP with anti-Myc Sepharose beads. (**E**) HEK293T cells were transiently transfected with Flag-tagged TRIM13, Myc-tagged STING, and hemagglutinin (HA)–tagged Ub (mutants) vectors as indicated for 48 hours. Then, polyubiquitination of immunoprecipitated STING was evaluated by Western blotting. (**F**) HEK293T cells were transiently transfected with Flag-tagged TRIM13, Myc-tagged STING (mutants), and HA-tagged Ub vectors as indicated for 48 hours. Then, polyubiquitination of immunoprecipitated STING was evaluated by Western blotting. One representative experiment of three is shown.

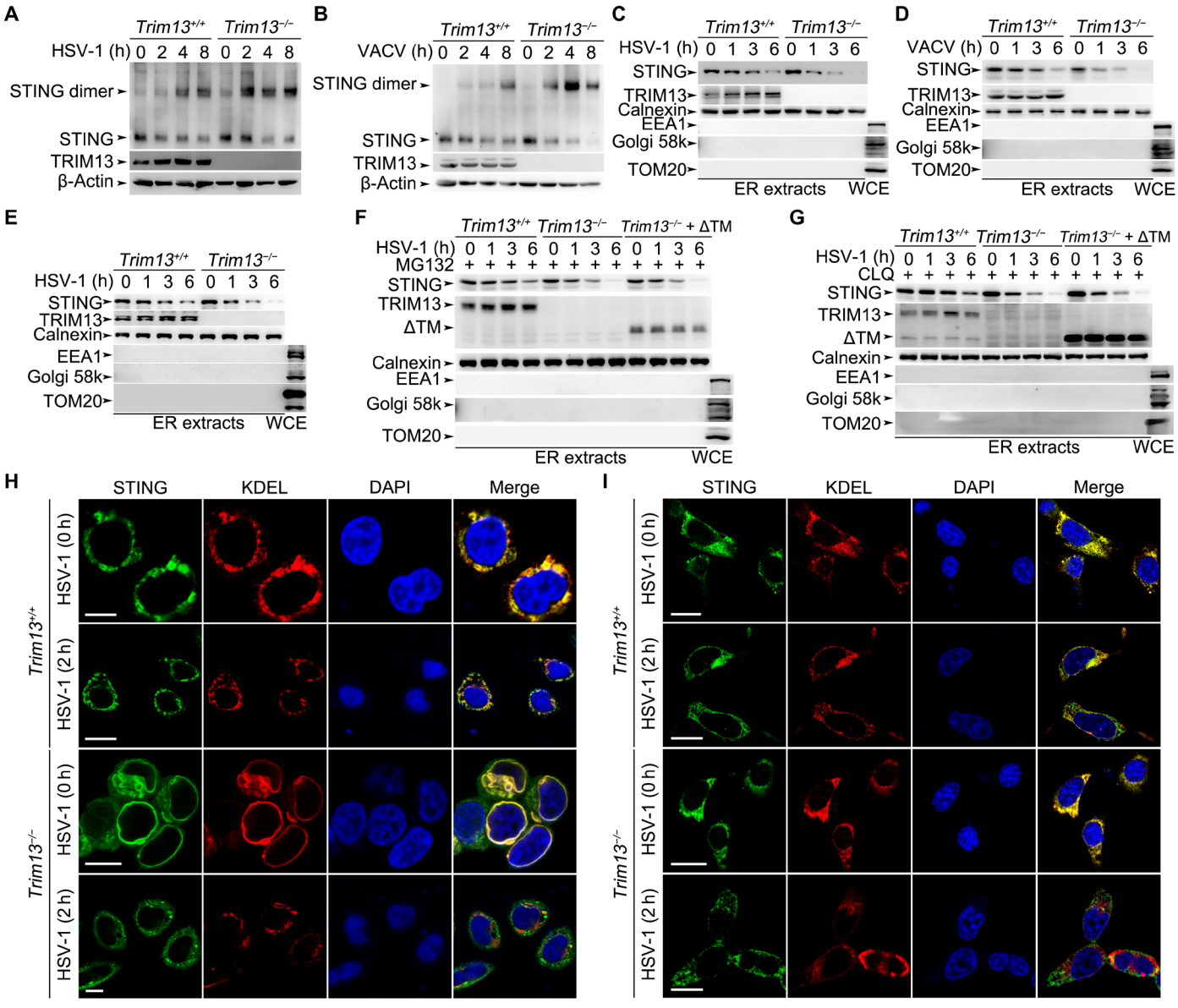

Fig. 6. TRIM13 inhibits STING dimerization and decelerates the ER exit of STING. (**A** and **B**) *Trim13*$^{+/+}$ or *Trim13*$^{-/-}$ BMDMs were infected with HSV-1 (MOI = 5) or VACV (MOI = 5) as indicated. Then, the nondenatured lysates were separated in native PAGE gel and then examined for STING by Western blotting. (**C** to **E**) ER extracts of *Trim13*$^{+/+}$ or *Trim13*$^{-/-}$ BMDMs (C and D) or MEFs (E) infected with HSV-1 (MOI = 5) or VACV (MOI = 5) as indicated were examined for STING by Western blotting. (**F** and **G**) *Trim13*$^{+/+}$ or *Trim13*$^{-/-}$ BMDMs were transfected with mock or TRIM13-ΔTM vectors for 48 hours and then infected with HSV-1 as indicated in the presence of 15 μM MG132 (F) or 20 μM chloroquine (CLQ) (G). ER extracts were examined by Western blotting. (**H** and **I**) *Trim13*$^{+/+}$ or *Trim13*$^{-/-}$ BMDMs (H) or MEFs (I) were infected with HSV-1 for 2 hours. Then, the colocalization of STING with KDEL was evaluated by confocal microscopy. Scale bars, 10 μm. One representative experiment of three is shown.

removal of STING from ER (Fig. 6F and fig. S9D). When the *Trim13*$^{-/-}$ BMDMs were rescued with TRIM13 without TM (TRIM13-ΔTM), the removal dynamic of STING could not be retrieved (Fig. 6F and fig. S9D). Previous studies have suggested that autophagosomal, autophagic, or lysosomal degradation of STING serves as termination module for STING degradation (*2*–*5*, *43*–*45*). So, we went further to use chloroquine (CLQ) to block the common terminal lysosomal STING degradation as reported (*43*–*45*). In the presence of CLQ, *Trim13*$^{-/-}$ BMDMs still demonstrated accelerated decrease of STING levels in ER (Fig. 6G and fig. S9E). These data indicate that the accelerated removal of STING from ER in TRIM13-deficient cells may not be solely because of STING degradation but possibly is caused by enhanced ER exit of STING.

To further validate the delayed exit of STING from ER, we performed colocalization assays using BMDMs and MEFs. In *Trim13*$^{-/-}$ cells, colocalization of STING with the ER marker KDEL after HSV-1 infection was more rapidly decreased within 2 hours when overall STING was minimally decreased (*43*, *44*), as compared to that in *Trim13*$^{+/+}$ cells (Fig. 6, H and I, and fig. S9, F and G). These data together suggest that TRIM13 may decelerate the ER exit of STING,

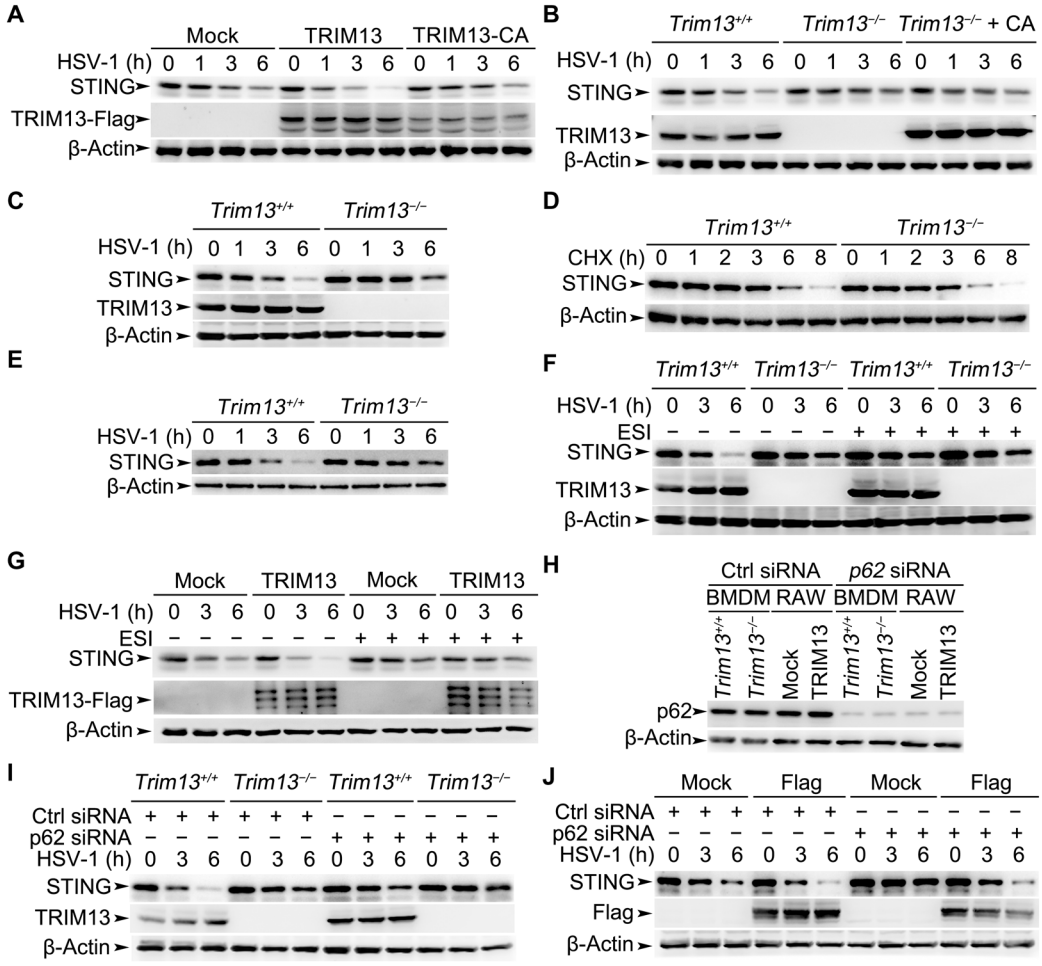

Fig. 7. TRIM13 promotes the degradation of STING. (**A**) RAW264.7 cells were transfected with indicated vectors for 48 hours. After HSV-1 infection, STING levels in WCE were examined by Western blotting (A). (**B** and **C**) BMDMs (B) or MEFs (C) were transfected with or without mock or TRIM13-CA vectors for 48 hours. STING levels were examined by Western blotting. (**D** and **E**) BMDMs were examined for STING degradation in the presence of CHX (20 μM) (D) or after pretreatment with CHX for 1 hour (E) by Western blotting. (**F** and **G**) *Trim13*$^{+/+}$ or *Trim13*$^{-/-}$ BMDMs (F) or RAW264.7 cells transfected with mock or TRIM13-Flag vectors for 48 hours (G) were infected with HSV-1 in the presence or absence of 20 μM ESI, and STING in WCE was examined by Western blotting. (**H** to **J**) RAW264.7 cells transfected with mock or TRIM13-Flag vectors for 48 hours (H and J) or *Trim13*$^{+/+}$ or *Trim13*$^{-/-}$ BMDMs (H and I) were transfected with control (Ctrl) siRNAs or p62-specific siRNAs for 48 hours. The efficiency of p62 knockdown was evaluated by Western blotting (H). STING in WCE was examined by Western blotting (I and J). One representative experiment of three is shown.

similarly to what has been reported for transmembrane STING regulators STIM1 and TMEM203 (*16*, *46*).

TRIM13 is required for STING degradation

We then determine what is the role of E3 ligase activity of TRIM13 in the inhibition of STING. In RAW264.7 cells, overexpression of TRIM13 accelerated the degradation of STING, while TRIM13-CA could not (Fig. 7A and fig. S10A). In *Trim13*$^{-/-}$ BMDMs and MEFs, we found that the overall STING amounts were increased, which could not be rescued by TRIM13-CA overexpression (Fig. 7, B and C, and fig. S10, B and C). To further confirm the role of TRIM13 in STING degradation, we performed the cycloheximide (CHX) chase assays for STING protein in BMDMs. We found that TRIM13 deficiency did not affect STING degradation in CHX-treated BMDMs without HSV-1 infection (Fig. 7D and fig. S10D), whereas the degradation of STING was delayed in CHX-pretreated *Trim13*$^{-/-}$ BMDMs after HSV-1 infection (Fig. 7E and fig. S10E). These data indicate that TRIM13 is required for DNA virus–induced STING degradation.

Because TRIM13 is durably localized in ER, it is possible that TRIM13 may regulate the degradation of STING through ER-initiated degradation (*47*, *48*), which may be different to ERGIC-initiated autophagosomal pathway and post-ER–initiated autophagic pathway (*43*–*45*). Given that TRIM13 has been implicated in ERAD of L-type calcium channels and CD3δ chain of T cell receptor (*35*, *36*), we investigated the effects of ERAD inhibitor Eeyarestatin I (ESI) on STING degradation. ESI-treated *Trim13*$^{+/+}$ BMDMs showed similar degradation dynamics to *Trim13*$^{-/-}$ cells without ESI treatments, while ESI treatments ameliorated the difference between *Trim13*$^{+/+}$ and *Trim13*$^{-/-}$ BMDMs in the degradation of STING (Fig. 7F and fig. S10F). Moreover, ESI treatments blocked TRIM13 overexpression–induced enhancement of STING degradation in RAW264.7 cells (Fig. 7G and fig. S10G). Therefore, TRIM13 mainly promotes STING degradation through ERAD pathway.

In addition to ERAD, another type of ER-initiated protein degradation is the autophagic degradation of the ER (termed as ER-phagy). TRIM13 has been implicated as a ubiquitin-dependent

ER-phagy receptor to p62 (*37*). So, it is possible that TRIM13 may promote ER-phagy degradation of STING (*49*). We knocked down p62 in BMDMs and RAW264.7 cells (Fig. 7H). *Trim13*$^{+/+}$ BMDMs with p62 knockdown showed similar degradation dynamics to *Trim13*$^{-/-}$ BMDMs without p62 knockdown, while p62 knockdown ameliorated the difference between *Trim13*$^{+/+}$ and *Trim13*$^{-/-}$ BMDMs in the degradation of STING (Fig. 7I and fig. S10H). Moreover, p62 knockdown could not reverse TRIM13 overexpression–induced STING degradation (Fig. 7J and fig. S10I). These data together suggest that ER-phagy may regulate STING degradation, while TRIM13 mainly promotes STING degradation through ERAD pathway.

The enhanced anti-DNA innate response by TRIM13 deficiency requires STING

To verify the role of STING in TRIM13-elicited inhibition of DNA-triggered inflammatory responses, we silenced the expression of STING (Fig. 8A) or inhibited the activation of STING by using C-176, a covalent small-molecule inhibitor for STING palmitoylation (*50*), in *Trim13*$^{-/-}$ BMDMs. We found that STING knockdown and C-176 both rescued the enhanced production of IFNβ and IL-6 by DNA viruses (Fig. 8, B to I), indicating that STING is required for TRIM13 deficiency–induced increase in cytokine production in response to DNA viruses.

To more specifically address the role of STING in TRIM13 loss–enhanced innate response to pathogenic DNAs, we prepared double-knockout (DKO; *Trim13*$^{-/-}$*Sting*$^{-/-}$) mice by breeding *Trim13*$^{-/-}$ mice with *Sting*$^{-/-}$ mice. In BMDMs treated with HSV-1 infection, we found that the DKO cells (Fig. 8J) showed similar levels of IFNβ and IL-6 to those of *Sting*$^{-/-}$ BMDMs (Fig. 8, K and L). Moreover, we found that the serum levels of IFNβ and IL-6 in DKO mice were similar to those in *Sting*$^{-/-}$ mice after HSV-1 infection (Fig. 8, M and N). The virus titers in the lung of DKO mice were not significantly different to that of *Sting*$^{-/-}$ mice (Fig. 8O). When the mice were pretreated with the STING inhibitor C-176, the virus titers in the lung of *Trim13*$^{-/-}$ mice were similar to *Trim13*$^{+/+}$ mice (Fig. 8P). These data confirm that STING is required for TRIM13 deficiency–induced enhancement of innate anti-DNA virus response.

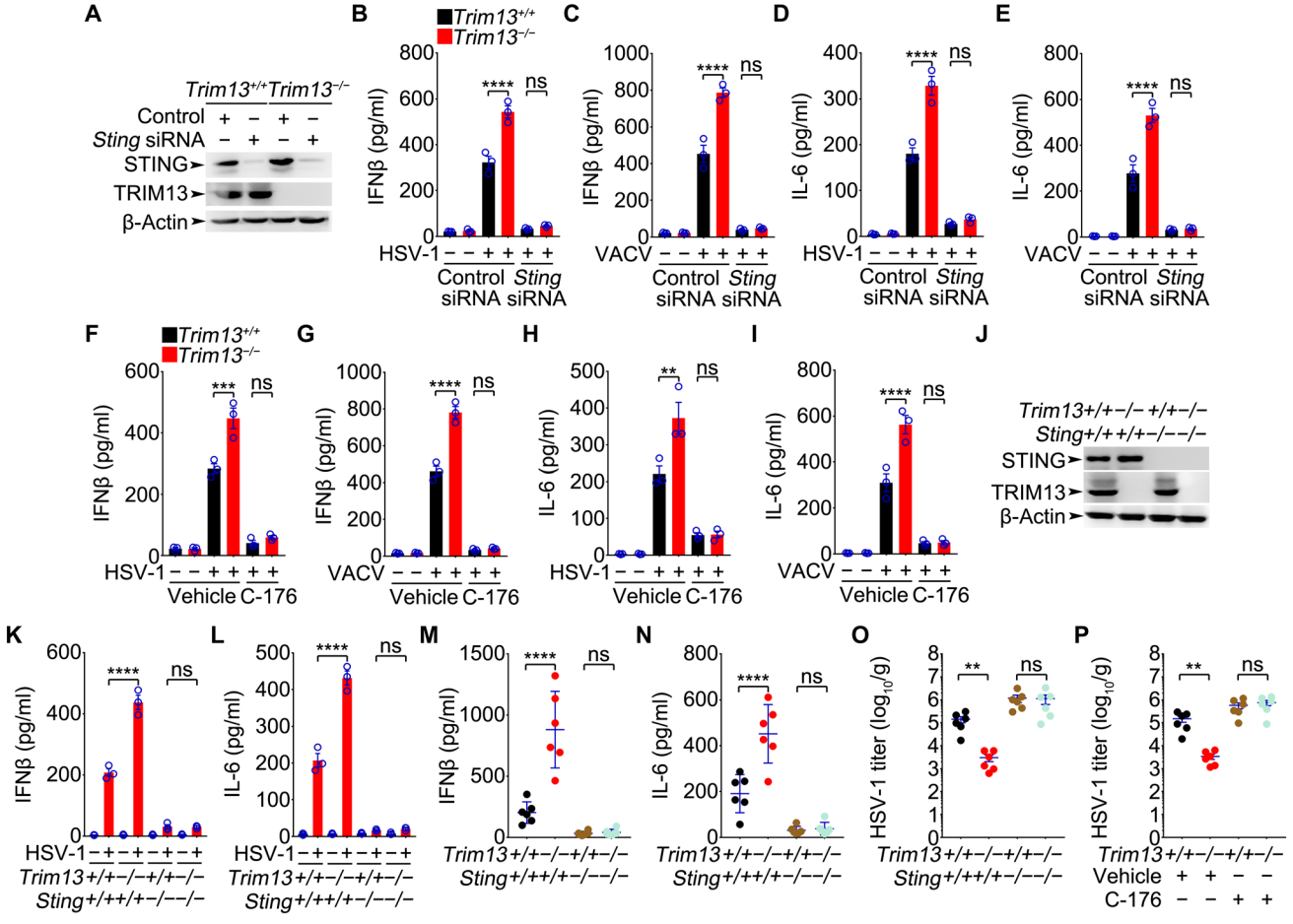

Fig. 8. STING is required for TRIM13 deficiency–induced enhanced innate anti-DNA response. (**A** to **I**) BMDMs ($n = 3$ mice) were transfected with siRNAs for 48 hours (A to E) and infected with viruses for 8 hours (B to E) in the presence or absence of 1 μM C-176 (F to I). The cytokines were measured by ELISA (B to I). (**J** to **O**) After infection of BMDMs (J) with HSV-1 for 8 hours (J to L), the cytokines were measured by ELISA (K and L) ($n = 3$ mice). Twelve hours later, after intraperitoneal injection of HSV-1 (2×10^8 PFUs), serum cytokines were measured by ELISA (M and N). Twenty-four hours after infections, the HSV-1 titers in the lung were determined (O). (**P**) *Trim13*$^{+/+}$ or *Trim13*$^{-/-}$ mice ($n = 6$) were pretreated with or without 300 nmol of C-176 daily for 2 days. Twenty-four hours after HSV-1 infection (2×10^8 PFUs), the HSV-1 titers in the lung were determined. Results (B to I and K to P) are presented as means ± SD (one-way ANOVA followed by Bonferroni multiple comparison). One representative experiment of three is shown. $^{**}P < 0.01$, $^{***}P < 0.001$, and $^{****}P < 0.0001$.

TRIM13 deficiency causes age-related autoinflammation in mice

Aberrant activation of STING has been linked to autoinflammatory or autoimmune diseases in human and mice (*12*, *13*), and the mutations of STING-interacting proteins, such as STIM1, TMEM203, and C9ORF72, have been implicated in autoinflammatory and autoimmune diseases (*16*, *46*, *51*). So, we wonder whether TRIM13 deficiency can also cause autoinflammatory symptoms in mice. Histological examination of organs, such as the lung, liver, kidney, heart, and brain, showed no marked inflammation signs in *Trim13*$^{-/-}$ mice at the age of 5 months (Fig. 9, A and B, and fig. S11, A to E). However, the 10-month-old *Trim13*$^{-/-}$ mice demonstrated extensive signs of inflammatory cell infiltrations in the lung, liver, and kidney and a mild infiltration of inflammatory cells in the heart and brain (Fig. 9, A and B, and fig. S11, A to E). Among the eight *Trim13*$^{-/-}$ mice examined by hematoxylin and eosin (H&E) staining, seven mice (87.5%) in the lung (around the bronchia or vessels), six mice (75.0%) in the kidney, four mice (50.0%) in the liver, one mouse (12.5%) in the brain, and one mouse (12.5%) in the heart showed foci of infiltrated inflammatory cells. Correspondingly, the amounts of IFNβ and IL-6 in the serum of 10-month-old *Trim13*$^{-/-}$ mice were significantly increased (Fig. 9C). Quantitative polymerase chain reaction (qPCR) assays of *Ifnb* and *Il6* in the lungs, livers, and kidneys of these *Trim13*$^{-/-}$ mice also demonstrated an increase of inflammatory cytokines (fig. S11, F and G). These data indicate that TRIM13 deficiency can cause age-related autoinflammation.

Immunofluorescence microscopy examination by staining CD45^{+} immune cells in the lung, liver, and kidney of 10-month-old mice confirmed that the observed inflammatory cell foci were composed of immune cells (Fig. 9D). We then further characterized the immune cells in the 10-month-old *Trim13*$^{-/-}$ mice by using immunofluorescence microscopy for immune cell markers. We found that the cells within the inflammatory cell foci were mainly composed of CD4^{+} and CD14^{+} cells; to a much lesser extent, CD8^{+} cells; and, minimally, F4/80^{+} or Ly6G^{+} cells (Fig. 9, E and F). However, TRIM13 deficiency did not affect the numbers of leukocytes, neutrophils, and lymphocytes in peripheral blood (fig. S12A). Moreover, the weight and major immune cell populations in the spleen of 10-month-old *Trim13*$^{-/-}$ mice were not significantly changed, as compared to *Trim13*$^{+/+}$ mice of the same age (fig. S12, B to D). These data indicate that the TRIM13 deficiency–initiated autoinflammation may be because of increased infiltration of inflammatory myeloid cells and CD4^{+} T cells.

As shown in Fig. 9E, most of the cells in the inflammatory foci of 10-month-old *Trim13*$^{-/-}$ mice were brightly stained for STING, indicating that STING levels may be increased in the tissues. So, we examined the lung tissues derived from 10-month-old *Trim13*$^{+/+}$ and *Trim13*$^{-/-}$ mice for STING, Caspase 8, MDA-5 (melanoma differentiation-associated gene 5), and NEMO (NF-κB essential modulator), all of which have been implicated as substrates for TRIM13 (*1*, *38*–*40*). Despite that STING levels were increased in the lung of *Trim13*$^{-/-}$ mice, TRIM13 deficiency did not affect the levels of the other potential substrates (fig. S13, A and B), indicating that STING may be the potential target for TRIM13 during age-related autoinflammation. Furthermore, we investigated whether the observed autoinflammatory changes in *Trim13*$^{-/-}$ mice were because of STING activation. When the 10-month-old *Trim13*$^{-/-}$ mice were treated with the STING inhibitor C-176, the serum levels of IFNβ and IL-6 (Fig. 9G) as well as the mRNA levels of *Ifnb* and *Il6* in the lungs (Fig. 9H) were all significantly reduced. These data suggest that TRIM13 deficiency–associated autoinflammation may be associated with STING activation.

As revealed in public database, mouse *Trim13* mRNA was highly expressed by macrophages. We wonder whether TRIM13 expressed by tissue-resident macrophages may contribute to the above-observed age-related autoinflammation in the lung. In the alveolar macrophages (AMs) derived from the BALFs of 8-week-old *Trim13*$^{-/-}$ mice, the production of inflammatory cytokines after HSV-1 infection or cGAMP treatment was enhanced (fig. S13, C to E). While the STING levels were comparable between *Trim13*$^{+/+}$ and *Trim13*$^{-/-}$ AMs before HSV-1 infection, the STING degradation was delayed in *Trim13*$^{-/-}$ AMs (fig. S13, F and G), which was consistent with that in BMDMs. However, in AMs derived from the BALFs of 10-month-old *Trim13*$^{-/-}$ mice, the levels of STING were increased (fig. S13, H and I), which may suggest that TRIM13 negatively regulates STING degradation in the presence of stimuli (possibly self-DNA in the current age-related experimental settings, as compared to AMs derived from 8-week-old mice). Meanwhile, the expression of inflammatory cytokines and chemokines for inflammatory cells was significantly higher in *Trim13*$^{-/-}$ AMs (fig. S13J), which may confer to the observed infiltration of inflammatory cells in the lungs in aged *Trim13*$^{-/-}$ mice and indicate that the tissue-resident macrophages may be one of the origins for the observed autoinflammation.

TRIM13 deficiency enhances double-stranded DNA–induced autoimmune response

We then determine whether TRIM13 deficiency can increase the sensitivity of mice to autoimmune diseases. In the GEO databases, it was demonstrated that human *Trim13* mRNA levels were significantly lower in peripheral blood monocytes and CD3^{+} T cells of patients with SLE (Fig. 10, A to C). In patients with MS, the *Trim13* mRNA levels were also significantly lower in brain lesions and peripheral blood mononuclear cells (PBMCs) (Fig. 10, D and E). Together, in the above age-related autoinflammatory data, it can be inferred that TRIM13 may contribute to the prevention of autoimmune diseases.

In the 10-month-old mice, we found that the concentrations of total immunoglobulin G (IgG) and IgM, and especially the levels of autoantibodies to nuclear antigen (ANA) and double-stranded DNA (dsDNA), were significantly higher in *Trim13*$^{-/-}$ mice than that in the age-matched *Trim13*$^{+/+}$ mice (Fig. 10, F to I), indicating that the aged *Trim13*$^{-/-}$ mice were prone to autoimmune diseases. To further explore the role of TRIM13 in autoimmunity, we immunized 8-week-old mice with dsDNA derived from autologous apoptotic thymocytes. Seven days after the second boost immunization, the levels of autoantibodies to dsDNA were significantly higher in mice with complete knockout of TRIM13 (crossed the *Trim13*$^{flox/flox}$ mice with EIIA-Cre mice, designated as *Trim13*$^{-/-}$) and in mice with myeloid-specific knockout of TRIM13 (crossed the *Trim13*$^{flox/flox}$ mice with Lyz-Cre mice, designated as *Trim13-Lyz*$^{-/-}$) (Fig. 10J), whereas the DKO mice (crossed the *Trim13*$^{-/-}$ mice or *Trim13-Lyz*$^{-/-}$ mice with *Sting*$^{-/-}$ mice) demonstrated similar amounts of serum anti-dsDNA autoantibody to that of *Sting*$^{-/-}$ mice (Fig. 10J). Therefore, TRIM13 deficiency may increase the sensitivity of host to autoimmune disease, which may require the presence of STING.

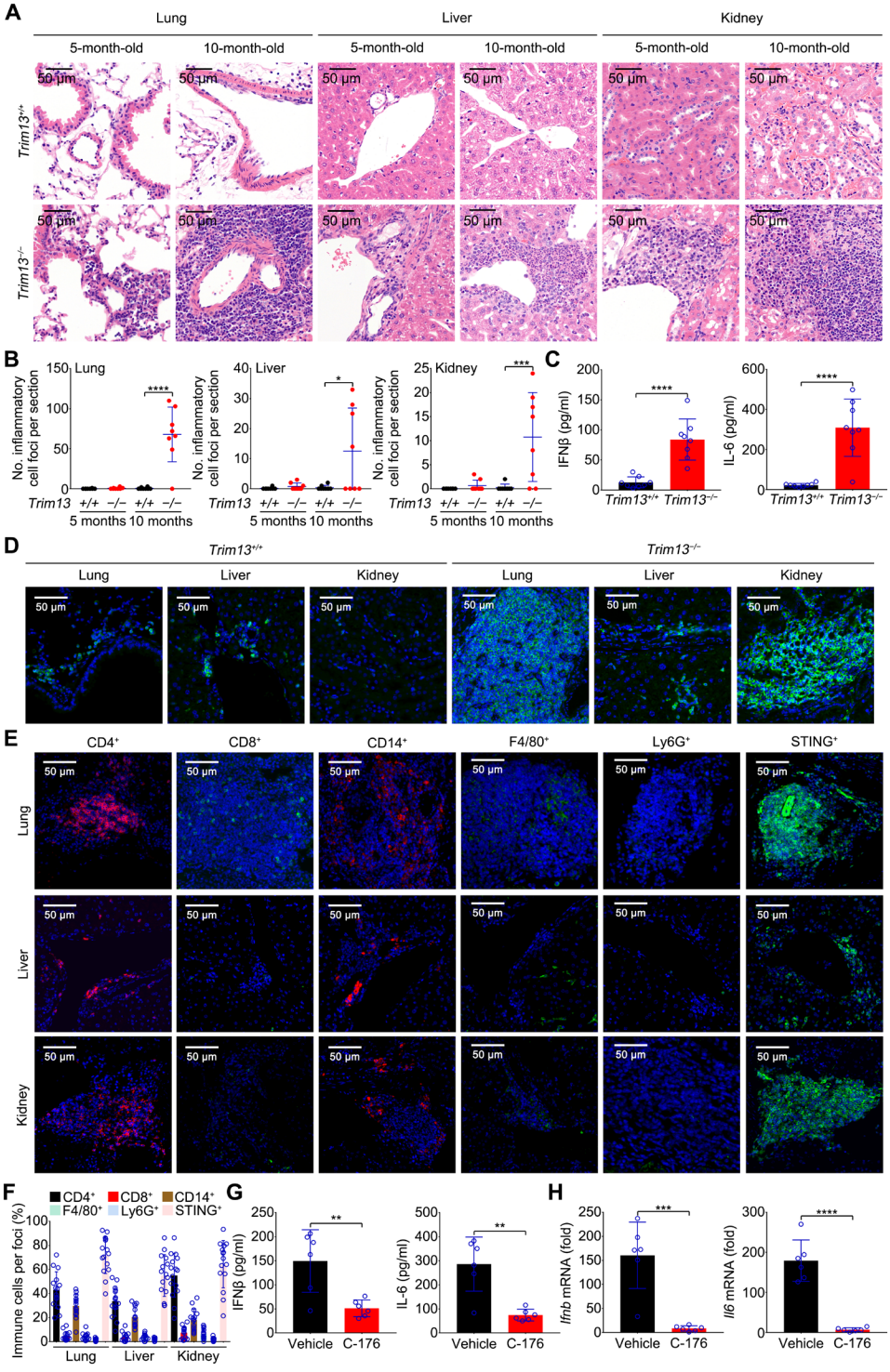

Fig. 9. TRIM13-deficient mice demonstrate age-related autoinflammation. (**A** and **B**) *Trim13*$^{+/+}$ or *Trim13*$^{-/-}$ mice were examined by H&E staining (A). The numbers of inflammatory cell foci (>30 cells per site) on each slide ($n = 8$ mice) were counted (B). (**C**) Serum cytokines of 10-month-old mice ($n = 8$) were measured by ELISA. (**D** to **F**) Tissues from 10-month-old *Trim13*$^{+/+}$ (D) or *Trim13*$^{-/-}$ mice (D to F) were stained for indicated immune cell markers [CD45^{+} in (D)] using an immunofluorescent microscope. The immune cell populations in 15 inflammatory foci ($n = 15$) of one slide were counted (F). (**G** and **H**) The 10-month-old *Trim13*$^{-/-}$ mice ($n = 6$) were pretreated with or without 300 nmol of C-176 daily for 10 days. Serum IFNβ and IL-6 were measured by ELISA (G). The mRNA levels of cytokines in the lung were quantified by qPCR (H). Results are presented as means ± SD (B, C, and F to H). [In (B), one-way ANOVA followed by Bonferroni multiple comparison; in (C), (G), and H, unpaired Student's *t* test]. One representative experiment of three is shown. *$P < 0.05$, **$P < 0.01$, ***$P < 0.001$, and ****$P < 0.0001$.

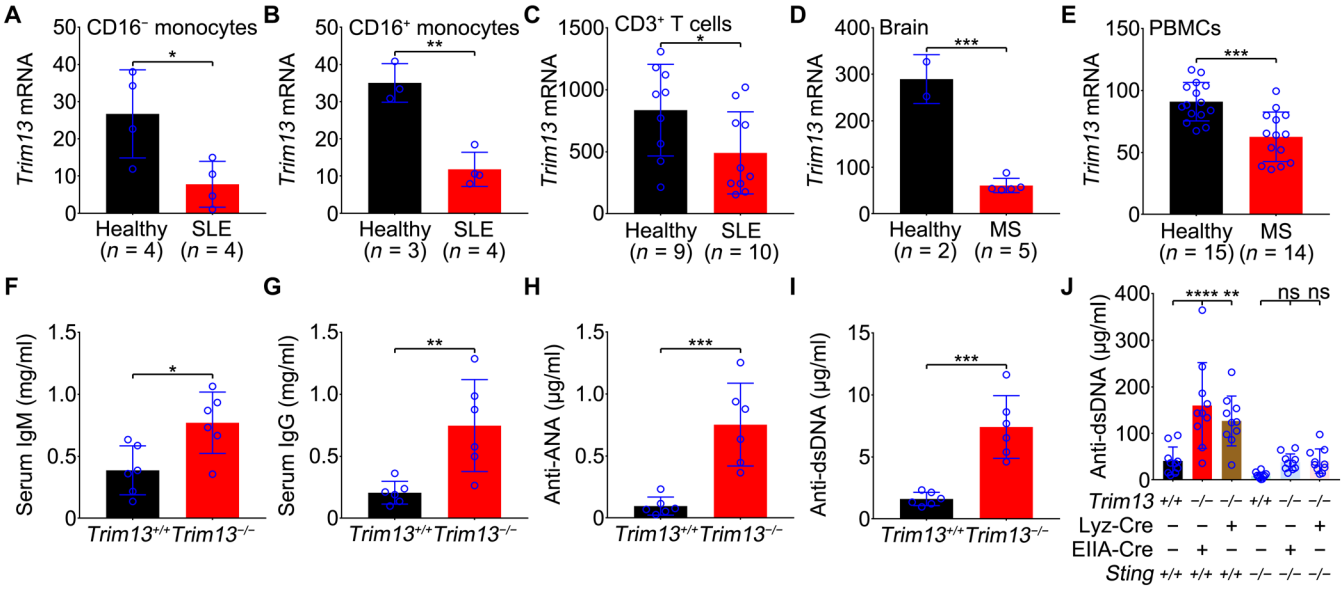

Fig. 10. TRIM13-deficient mice demonstrate enhanced anti–double-stranded DNA (dsDNA) autoimmune response. (**A** to **E**) Data derived from the GEO databases were analyzed for differential *Trim13* mRNA expression. The datasets cited were GDS4889 (A), GDS4890 (B), GDS4719 (C), GDS4218 (D), and GDS3920 (E). (**F** to **I**) Total immunoglobulin M (IgM) (F) and IgG (G) as well as autoantibodies against autoantibodies to nuclear antigen (ANA) (H) and dsDNA (I) in the serum of 10-month-old $Trim13^{+/+}$ or $Trim13^{-/-}$ mice ($n = 6$ mice per group) were measured by ELISA. (**J**) 8-week-old mice ($n = 6$ per group) were immunized for genomic DNA derived from autologous apoptotic thymocytes. Seven days after the second boost, autoantibodies against dsDNA in the serum were measured by ELISA. Results are presented as means ± SD of indicated biological samples (A to I, unpaired Student's *t* test; J, one-way ANOVA followed by Bonferroni multiple comparison). One representative experiment of three is shown. $^{*}P < 0.05$, $^{**}P < 0.01$, $^{***}P < 0.001$, and $^{****}P < 0.0001$.

DISCUSSION

Our study demonstrates the negative role of TRIM13 in restraining STING activation in response to pathogenic DNAs by using knockout models. Moreover, we show that TRIM13 is critical in regulating STING homeostasis during innate immune response to pathogenic DNAs. Age-related autoinflammation observed in TRIM13 knockout mice supports a proposal for the important role of TRIM13 in inflammatory diseases.

The activation of STING should be tightly controlled for prevention of autoinflammatory and autoimmune diseases. Patients bearing gain-of-function mutations in the STING-encoding gene *Tmem173*, such as V147L, N154S, and V155M, demonstrated symptoms called SAVI, mainly manifesting skin, mucosa, and lung inflammation (*12*, *13*). These mutations in STING led to STING traffic from the ER in the absence of cGAMP and transit through the ERGIC and Golgi apparatus (*52*). The knock-in mice containing N153S or V154M mutations of murine STING demonstrated severe perivascular inflammation in the lung and skin, which may be caused by myeloid cell expansion, T cell cytopenia, and disruption of lymph node organogenesis and innate lymphoid cell development (*2*–*5*, *13*, *53*–*58*). In our study, TRIM13 knockout mice show signs of age-related autoinflammation and autoimmunity at the age of 10 months, unlike the early onset of autoinflammation in STING-mutated mice. The symptoms observed in TRIM13 knockout mice partially resemble to, but were less severe in terms of organ-involved and onset age than, those in STING-mutated mice (*2*–*4*, *13*, *53*–*58*). Whether the autoinflammation in TRIM13-null aged mice is caused by STING activation has not been completely validated by our study. Our study provides evidence for the critical role of STING in TRIM13 deficiency–caused enhancement of innate inflammatory response to DNA virus by using STING knockdown, STING inhibitor C-176, and DKO models. STING knockout that ameliorates the autologous DNA-induced autoantibody production in $Trim13^{-/-}$ mice may further support the functional linkage between TRIM13 and STING. The ideal evidence may be the confirmation of reversed autoinflammatory symptoms in the aged DKO mice, which, because of time-consuming experiments, have not been obtained at present but would be a notice to us in future studies. On the other hand, it is still not clear whether TRIM13 deficiency–caused age-related autoinflammation was dependent on type I IFN or T cell cytopenia. Our preliminary phenotyping of immune cells in the spleen of 10-month-old $Trim13^{-/-}$ mice may indicate that TRIM13 may not severely affect the numbers of major immune cell populations, which was unlike to what had been reported for STING-mutated mice (*2*–*5*, *13*, *53*–*58*). Future studies using knockout aged mice, such as STING, IRF3, or IFNα receptor knockout mice as well as conditional T cell–specific knockout mice, may help to resolve this concern. As indicated in public databases, murine STING is widely expressed in many cells, especially high in T cells, B cells, natural killer cells, dendritic cells, and macrophages, whereas *Trim13* mRNA was relatively restricted in macrophages and low in T cells and B cells, which may contribute to the observed differential symptoms between the STING-mutated mice and the aged TRIM13-deficient mice. The data from experiments in aged AMs may propose that tissue-resident macrophages may be the driver for infiltrated inflammatory cells, given that self-DNA is usually increased in aged mice and chemokines are induced in the AMs of autoinflammatory $Trim13^{-/-}$ mice. Another possibility for the later onset of autoinflammation in $Trim13^{-/-}$ mice is that TRIM13 deficiency may be compensated partially by the other negative STING regulators, such as E3s and STING-associated proteins (*2*–*5*, *14*–*26*, *46*, *51*), when the mice are healthy and young.

Correspondingly, the STING levels in healthy adult mice or in resting macrophages were comparably between *Trim13*$^{+/+}$ and *Trim13*$^{-/-}$ genotypes, while the STING proteins were increased in aged autoinflammatory *Trim13*$^{-/-}$ mice, indicating a relatively specific requirement for TRIM13 in STING homeostasis under the condition of pathogenic-DNA stimuli. Whether TRIM13 is involved in the development or functional regulation of T cells (e.g., T helper 17 cells, innate lymphoid cells, etc.) and B cells awaits elaborate studies in the future.

STING is an ER-associated adaptor for innate response to pathogenic DNAs (*2*–*5*). CDN or cGAMP triggers STING dimerization and then the exit from ER in the form of COP-II (coat protein complex II) vesicles and ERGIC (*2*–*5*). Part of the ERGIC-associated STING is sorted into autophagosomes, while the other vesicle-associated STING continues to transit to Golgi and post-Golgi vesicles where the signalosome composed of STING, TBK1, and IRF3 is formed (*2*–*5*, *59*). TBK1 recruited by STING phosphorylates STING at several sites and amplifies the activation of TBK1 and IRF3, leading to the induction of inflammatory cytokines and ISGs (*59*, *60*). Recent studies have also proposed IFN-independent and transcription-independent functions for STING during antiviral process (*45*, *61*, *62*). Along the STING activation pathways, multiple negative mechanisms have been identified to restrain STING signaling. ER exit of STING is the initial rate-limiting step for which STIM1 has been proposed to delay ER exit to ERGIC and inhibit dimerization of STING by interaction with TM of STING (*16*). TRIM13 is a transmembrane ER-associated molecule and can interact with STING through TM, which is similar to the reported STIM1-STING interaction (*16*). Therefore, it may be reasonable to find that TRIM13 delays the ER exit of STING and inhibits STING dimerization in our study. It will be interesting to explore whether TRIM13 can interact with STIM1 in the future. After ER exit, assembly of STING signalosome in ERGIC, Golgi apparatus, and possibly endolysosomes is another step under tight control through posttranslational modification or competitive interaction with STING (*2*–*5*, *14*, *15*, *17*, *18*, *24*, *25*). Because TRIM13 can delay the ER exit of STING and, itself, is constitutively localized to ER, it may not directly affect the STING signalosome formation. Degradation of STING serves as the most popular and final feedback mechanisms for termination of STING signaling. ULK1 and ATG9a promote autophagic degradation of STING, while p62 directly targets ubiquitinated STING to autophagosomes (*2*–*5*, *17*, *26*, *43*–*45*). E3 ubiquitin ligases RNF5, TRIM29, and TRIM30a mark STING for proteasomal degradation (*20*–*23*). The STING-interacting partners TMEM203 and C9ORF72 promote the degradation of STING through facilitating lysosomal and autolysosomal pathways (*46*, *51*). ER-phagy may also serve as a potential STING degradation pathway (*49*), which has not been clearly understood. TRIM13 promotes degradation of STING after DNA virus infection, as evidenced by extensive Western blotting assays and quantification assays using *Trim13*$^{-/-}$ BMDMs and MEFs or after TRIM13 overexpression in macrophages. The stable localization of TRIM13 in ER supports a proposal for ER-initiated degradation, which may be different to ERGIC-initiated autophagosomal, autophagic, or lysosomal degradation pathways because these pathways require the ER exit of STING. Currently, ERAD and ER-phagy are the known ER-initiated protein degradation mechanisms (*47*, *48*). Our data suggest that TRIM13 may facilitate STING degradation via the ERAD pathway because ERAD inhibitor ESI completely ameliorated the differences in dynamics of STING degradation between *Trim13*$^{+/+}$ and *Trim13*$^{-/-}$ cells as well as between mock-transfected and TRIM13-overexpressed cells. Although TRIM13 has been implicated in the process of ER-phagy (*37*), p62 knockdown could not completely reverse the effects of TRIM13 on STING degradation. However, p62 has been widely implicated in multiple protein degradation pathways, including, but not limited to, autophagosomal, autophagic, lysosomal, proteasomal, ER-associated, and ER-phagic degradation pathways (*47*, *48*). So, it cannot be excluded that TRIM13 may also affect STING degradation through other pathways (especially ER-phagy), which may require more accurate protein quantification technique in except of Western blotting. On the basis of these considerations, we propose that TRIM13 restrains STING-related innate response to pathogenic DNAs by modulating ER exit and degradation of STING.

E3 ligases and deubiquitinases can add or remove different types of ubiquitin chains from STING and regulate STING activation or stability. Various types of polyubiquitination on different sites of STING have been identified, such as Lys^{48} linkage (Lys^{150} by RNF5, Lys^{370} by TRIM29, and Lys^{275} by TRIM30a), Lys^{63} linkage (Lys^{150} by TRIM56, Lys^{224} by MUL1, and Lys$^{20/150/224/236}$ by TRIM32), Lys^{11} linkage (Lys^{150} by RNF26), and Lys^{27} linkage (Lys$^{137/150/224/236}$ by AMFR) (*2*–*5*, *20*–*23*, *28*–*32*). However, Lys^{6}, Lys^{29}, and Lys^{33} types of STING polyubiquitinations have not been reported. Our study identifies a previously unidentified type of STING polyubiquitination, Lys^{6}-linked polyubiquitination. Whether this type of ubiquitylation is related or specific to ERAD is not clear and awaits further studies. Lys^{19} (Lys^{20} in human) is the first Lys residue in STING located just before the first TM- of STING. TRIM32 catalyzes Lys^{63}-linked polyubiquitination on this residue and facilitates STING interaction with TBK1 (*29*). TRIM13 catalyzes Lys^{6} linkage on Lys^{19} of STING and directs STING for degradation, leading to inhibited STING activation instead. TRIM13 is structurally alike to RNF5 in containing TM-, and both are of abundant expression in macrophages. RNF5 can be localized in both ER and mitochondria and mediates RNA virus–induced degradation of STING and MAVS (mitochondrial antiviral signaling protein) while its role in innate anti-DNA virus has not been verified (*20*, *63*). RNF5 has also been implicated in ERAD of STING (*64*). Previously, TRIM13 has been reported to inhibit RNA virus–induced inflammatory response possibly through MDA-5 (*40*). Whether TRIM13 regulates anti-RNA virus innate response through ERAD may warrant future investigations. Therefore, TRIM13 catalyzes a previously unidentified type of STING polyubiquitination, which serves as a negative mechanism for controlling STING activation.

In summary, our study has provided genetic evidence for the critical role of TRIM13 in retraining STING activation in response to pathogenic DNAs. The Lys^{6}-linked polyubiquitination of STING by TRIM13 serves as an important marker for STING degradation, providing a potential brake for STING activation. TRIM13 deficiency–associated age-related autoinflammation strongly encourages further exploration into the potential significance of TRIM13 in human autoinflammatory and autoimmune diseases.

MATERIALS AND METHODS

Mice and cells

All animal experiments were undertaken in accordance with the National Institute of Health Guide for the Care and Use of Laboratory Animals, with the approval of the Scientific Investigation Board of the Second Military Medical University, Shanghai. C57BL/6

(H-2K^b) WT mice (6 to 8 weeks of age) were purchased from Joint Ventures Sipper BK Experimental Animal (Shanghai, China). The *Trim13* conditional knockout mice were established by using a recombinant strategy through replacing exon 3 of *Trim13* with insertion of LoxP sequence at both ends with the assistance of the Shanghai Model Organisms Center Inc. (Shanghai, China) as described (*65*, *66*) and were backcrossed with C57BL/6 mice for more than six generations. The *Trim13*$^{flox/flox}$ mice were crossed with EIIA-Cre mice or Lyz-Cre mice to create complete knockout or myeloid-specific knockout mice for experiments. The C57BL/6N-Sting1^{em1cyagen} (*Sting*$^{-/-}$ mice; strain code KOCMP-72512-Sting1-B6N-VA) were purchased from Cyagen (Guangdong, China). For genotyping of mice, tail DNA was extracted, and PCR was performed as described (*65*, *66*). The genotyping primer sequences and the standards are described in table S2.

The HeLa, HEK293T, and RAW264.7 cells were obtained from and authenticated by the American Type Culture Collection (ATCC; Manassas, VA) and were cultured as suggested by the supplier. PMs and BMDMs were prepared and cultured as described previously (*42*, *65*, *66*). For the isolation of AMs from murine BALFs, after perfusion of the lung by injecting 10 ml of ice-cold phosphate-buffered saline (PBS) into the right ventricle for three times, the BALFs were collected (1 ml each time for a total of 10 times). Then, the cells in BALFs were obtained by centrifugation at 300*g* for 10 min. After adhesion on plastic dishes for 2 hours, the nonadherent cells were washed off, while the remaining adherent cells were taken as AMs [more than 90% of the cells were F4/80 positive as examined by FACS (fluorescence-activated cell sorting)]. For the depletion of mouse STING in RAW264.7 cells, pc3-U6-guide RNA-CMV-RED (encoding guiding RNA and RFP) and Cas9-IRES-EGFP [encoding Cas9 and green fluorescent protein (GFP)] plasmids (gifts from the Shanghai Model Organisms Center Inc., Shanghai, China) were cotransfected into RAW264.7 cells as described (*42*). Cells with both red and green fluorescence were then sorted by using the Gallios Flow Cytometer (Beckman Coulter, Brea, CA). Sorted cells were cultured for 3 to 5 days, and clones propagated from single cell were picked out. Three target sequences for guiding RNA synthesis against *Sting* were designed (table S2). The embryonic day 13.5 (E13.5) MEFs derived from *Trim13*$^{+/+}$ or *Trim13*$^{-/-}$ mice were prepared as described previously (*67*).

Antibodies, reagents, and viruses

The antibodies and major reagents used in this study are listed in table S3. HSV-1 (F strain; a gift from Q. Li, Chinese Academy of Medical Sciences, China) and VACV (ATCC, Manassas, VA) were propagated in the monolayer of Vero cells. For infection in vitro, cells were infected with HSV-1 [multiplicity of infection (MOI) = 5] or VACV (MOI = 5), respectively. Poly (dA:dT) (5 μg/ml) and 3′,3′-cGAMP (5 μg/ml) were from InvivoGen (San Diego, California). Other nonspecified reagents were purchased from Sigma-Aldrich (St. Louis, MO).

Plasmids, transfection, and RNA interference

The recombinant vectors encoding mouse TRIM13 (GenBank, no. NM_001164220.1) and STING (GenBank, no. NM_028261.1) as well as the indicated mutations were constructed as described (*42*, *65*, *66*). For transient transfection of plasmids in RAW264.7 and HEK293T cells, the X-tremeGENE HP reagents were used according to the manufacturer's instructions (Roche, Welwyn Garden City, UK). For transient knockdown of *Trim13*, three siRNA duplexes for mouse or human *Trim13* were synthesized (table S2) and transfected using the INTERFERin-HTS according to the standard protocol (Polyplus-transfection Company, Illkirch, France). The siRNA duplexes specific for *Sting* (sc-154411) and *p62* (sc-35233) were obtained from Santa Cruz Biotechnology (Dallas, TX). siRNA sequences specific for *Rnf5*, *Trim29*, and *Trim30a* are listed in table S2. The nonsense sequence 5′-TTCTCCGAACGTGTCACG-3′ was used as control siRNA.

Quantitative polymerase chain reaction

Total cellular RNA was extracted using TRIzol reagent (Invitrogen Corporation, CA, USA), and cDNA was synthesized by using the AMV (avian myeloblastosis virus) Reverse Transcriptase Kit (Promega, Madison, WI). The mRNA quantification methods were as described (*42*, *65*, *66*). The primer sequences are listed in table S2.

Enzyme-linked immunosorbent assay of cytokines

Enzyme-linked immunosorbent assay (ELISA) kits for mouse IFNβ, TNF, and IL-6 were from R&D Systems (Minneapolis, MN). The concentrations of cytokines in the culture supernatants or serum were determined as recommended by the manufacturer.

Nanospray LC–tandem mass spectrometry

The identification of the TRIM13-associated proteins was performed as described previously (*42*, *65*, *66*). The nano-ultraperformance LC electrospray ionization tandem mass spectrometry was performed by the Beijing Genomics Institute (Beijing, China).

Luciferase assays

The NF-κB and *Ifnb* luciferase reporter plasmids were obtained from Panomics of Affymetrix (Santa Clara, CA). Luciferase activities were measured with the Dual-Luciferase Reporter Assay System (Promega, Madison, WI). The determination of reporter transactivation was performed as described previously (*42*, *66*).

IP and immunoblot

The IP using anti-TRIM13, anti-STING, anti-Flag, or anti-Myc antibodies and the immunoblot assays were performed as described previously (*42*, *66*). The quantification of protein bands from Western blotting was performed using the ImageJ software.

Immunofluorescence confocal microscopy

RAW264.7 cells, MEFs, or HeLa cells seeded on cover sliders were transiently cotransfected with TRIM13-RFP or STING-GFP vectors for 48 hours. Samples were washed briefly in PBS and fixed in 4% paraformaldehyde. For colocalization assays of TRIM13 or STING with organelle markers, cells were permeabilized in blocking buffer containing 0.5% saponin and then sequentially stained with anti-KDEL, EEA1, TOM20 or Golgi 58K, and Oregon Green 488–conjugated secondary antibody. Upon confocal microscopy, cells were immediately stained with DAPI (4′,6-diamidino-2-phenylindole) (10 μg/ml) and covered by cover glasses. Images were obtained with a laser scanning confocal microscope (Leica TCS SP8) and analyzed by the LAS X software version 2.0.2.15022.

Polyubiquitination assays

For the examination of polyubiquitination of STING, cells were lysed in stringent lysis buffer supplemented with 1% Triton X-100, 1% NP-40, and 300 mM NaCl. Lysates were denatured by heat in

1% SDS, followed by IP with anti-STING antibody and protein A/G beads. The pellets were extensively washed for four times with the lysis buffer. Then, the final pellets were resolved in SDS sample buffer, and the ubiquitination of STING was examined by Western blot (*42*, *66*).

ER isolation

The ER fractions were purified using the Endoplasmic Reticulum Isolation Kit (#ER0100, Sigma-Aldrich) as recommended and as described (*68*). BMDMs, MEFs, or RAW264.7 cells from five 15-cm dishes were collected and homogenized by passing through a 22-gauge needle until ~85% lysis. The homogenates were centrifuged sequentially at 1000*g* for 10 min, at 12,000*g* for 15 min, and at 100,000*g* for 1 hour. The pellets (crude microsome) were resuspended in 1× isotonic extraction buffer [10 mM Hepes (pH 7.8), 250 mM sucrose, 25 mM potassium chloride, and 1 mM EGTA] and were loaded onto a 15 to 23% OptiPrep gradient and ultracentrifuged for 18 hours at 80,000*g*. Immunoblotting was applied to identify the fraction(s) most enriched for ER. For quality control, calnexin was used as positive control, while TOM20, EEA1, and Golgi 58K were used as negative control.

Animal models and manipulations

Age- and gender-matched mice with indicated genotype were used to establish animal models. For in vivo infection with pathogens, mice were intraperitoneally injected with 100 μl of PBS containing 2×10^8 or 5×10^8 PFUs of HSV-1. To mimic the neural infection of HSV-1, 100 μl of PBS containing 2×10^8 PFUs of HSV-1 was intravenously injected via tail vein. The microbe titers in the liver, spleen, lung, and brain were determined by qPCR assays of *Icp0* mRNA of HSV-1 or by plaque formation assays as described previously (*42*, *65*).

For the examination of inflammation in organs, mice were anesthetized intraperitoneally with pentobarbital (50 mg/kg), extracted for blood from the eyeballs, euthanized by cervical dislocation, and flushed via the right ventricle with 15 ml of sterile PBS. The liver, lung, kidney, brain, and heart were excised, fixed in 4% formalin, embedded in paraffin, cut into 4-μm sections, affixed onto glass slides, deparaffinized, and stained with H&E. Peribronchial and perivascular inflammation were scored by counting the number of inflammatory cell foci (>30 cells per site) on each slide under ×2 magnification of light microscopy. The immune cell subsets in the foci were characterized by immunofluorescence microscopy as described previously (*66*), and the fluorescent antibodies are listed in table S3. To treat the autoinflammation, the 10-month-old *Trim13*$^{-/-}$ mice were intraperitoneally injected with 300 nmol of C-176 in 150 μl of corn oil or corn oil alone daily for 10 days.

To explore the potential linkage between TRIM13 and autoimmune symptoms, the serum levels of IgG and IgM were quantified by using mouse IgM (ab133047) and IgG (ab151276) ELISA kit from Abcam (Cambridge, MA) as recommended. Autoantibodies against ANA (ABIN772680) and dsDNA (ABIN627743) in serum were measured by using ELISA kit from Antibodies-online Ltd. (Aachen, Germany).

For the dsDNA immunization experiments, 8-week-old mice with indicated genotypes were immunized subcutaneously with genomic DNA (50 mg per mouse; derived from apoptotic thymocytes after 10 μM dexamethasone treatments for 48 hours) plus Freund's complete adjuvant (Sigma-Aldrich) on day 1, followed by subcutaneous injection of apoptotic thymocyte DNA (50 mg per mouse) emulsified with incomplete Freund's adjuvant (Sigma-Aldrich) on days 14 and 28 for a total of two boosts. Serum samples were collected 7 days later for ELISA assays of anti-dsDNA antibody.

Statistical analysis

All the experiments were independently repeated at least two or three times. Results are given as means ± SE or means ± SD. Sample sizes were chosen by standard methods to ensure adequate power and no exclusion. Comparisons between two groups were done using two-tail unpaired Student's *t* test. Multiple comparisons were done with one-way analysis of variance (ANOVA) followed by Bonferroni multiple comparisons. The survival of mice was monitored by Kaplan and Meier method and analyzed by log-rank test. Statistical significance was determined as $P < 0.05$. All the statistics were performed using the software GraphPad Prism 7.0.

SUPPLEMENTARY MATERIALS

Supplementary material for this article is available at https://science.org/doi/10.1126/sciadv.abh0496

View/request a protocol for this paper from *Bio-protocol*.

REFERENCES AND NOTES

1. X. Cao, Self-regulation and cross-regulation of pattern-recognition receptor signalling in health and disease. *Nat. Rev. Immunol.* **16**, 35–50 (2016).
2. X. Zhang, X. C. Bai, Z. J. Chen, Structures and mechanisms in the cGAS-STING innate immunity pathway. *Immunity* **53**, 43–53 (2020).
3. K. P. Hopfner, V. Hornung, Molecular mechanisms and cellular functions of cGAS-STING signalling. *Nat. Rev. Mol. Cell Biol.* **21**, 501–521 (2020).
4. M. Motwani, S. Pesiridis, K. A. Fitzgerald, DNA sensing by the cGAS-STING pathway in health and disease. *Nat. Rev. Genet.* **20**, 657–674 (2019).
5. A. Decout, J. D. Katz, S. Venkatraman, A. Ablasser, The cGAS-STING pathway as a therapeutic target in inflammatory diseases. *Nat. Rev. Immunol.* **8**, 1–22 (2021).
6. L. Wang, M. Wen, X. Cao, Nuclear hnRNPA2B1 initiates and amplifies the innate immune response to DNA viruses. *Science* **365**, eaav0758 (2019).
7. H. Ishikawa, G. N. Barber, STING is an endoplasmic reticulum adaptor that facilitates innate immune signalling. *Nature* **455**, 674–678 (2008).
8. H. Ishikawa, Z. Ma, G. N. Barber, STING regulates intracellular DNA-mediated, type I interferon-dependent innate immunity. *Nature* **461**, 788–792 (2009).
9. B. Zhong, Y. Yang, S. Li, Y. Y. Wang, Y. Li, F. Diao, C. Lei, X. He, L. Zhang, P. Tien, H. B. Shu, The adaptor protein MITA links virus-sensing receptors to IRF3 transcription factor activation. *Immunity* **29**, 538–550 (2008).
10. W. Sun, Y. Li, L. Chen, H. Chen, F. You, X. Zhou, Y. Zhou, Z. Zhai, D. Chen, Z. Jiang, ERIS, an endoplasmic reticulum IFN stimulator, activates innate immune signaling through dimerization. *Proc. Natl. Acad. Sci. U.S.A.* **106**, 8653–8658 (2009).
11. L. Jin, P. M. Waterman, K. R. Jonscher, C. M. Short, N. A. Reisdorph, J. C. Cambier, MPYS, a novel membrane tetraspanner, is associated with major histocompatibility complex class II and mediates transduction of apoptotic signals. *Mol. Cell. Biol.* **28**, 5014–5026 (2008).
12. Y. Liu, A. A. Jesus, B. Marrero, D. Yang, S. E. Ramsey, G. A. M. Sanchez, K. Tenbrock, H. Wittkowski, O. Y. Jones, H. S. Kuehn, C. R. Lee, M. A. DiMattia, E. W. Cowen, B. Gonzalez, I. Palmer, J. J. DiGiovanna, A. Biancotto, H. Kim, W. L. Tsai, A. M. Trier, Y. Huang, D. L. Stone, S. Hill, H. J. Kim, C. S. Hilaire, S. Gurprasad, N. Plass, D. Chapelle, I. Horkayne-Szakaly, D. Foell, A. Barysenka, F. Candotti, S. M. Holland, J. D. Hughes, H. Mehmet, A. C. Issekutz, M. Raffeld, J. McElwee, J. R. Fontana, C. P. Minniti, S. Moir, D. L. Kastner, M. Gadina, A. C. Steven, P. T. Wingfield, S. R. Brooks, S. D. Rosenzweig, T. A. Fleisher, Z. Deng, M. Boehm, A. S. Paller, R. Goldbach-Mansky, Activated STING in a vascular and pulmonary syndrome. *N. Engl. J. Med.* **371**, 507–518 (2014).
13. Y. J. Crow, N. Manel, Aicardi-Goutières syndrome and the type I interferonopathies. *Nat. Rev. Immunol.* **15**, 429–440 (2015).
14. H. Guo, R. König, M. Deng, M. Riess, J. Mo, L. Zhang, A. Petrucelli, S. M. Yoh, B. Barefoot, M. Samo, G. D. Sempowski, A. Zhang, A. M. Colberg-Poley, H. Feng, S. M. Lemon, Y. Liu, Y. Zhang, H. Wen, Z. Zhang, B. Damania, L. C. Tsao, Q. Wang, L. Su, J. A. Duncan, S. K. Chanda, J. P. Ting, NLRX1 sequesters STING to negatively regulate the interferon response, thereby facilitating the replication of HIV-1 and DNA viruses. *Cell Host Microbe* **19**, 515–528 (2016).
15. L. Zhang, J. Mo, K. V. Swanson, H. Wen, A. Petrucelli, S. M. Gregory, Z. Zhang, M. Schneider, Y. Jiang, K. A. Fitzgerald, S. Ouyang, Z. J. Liu, B. Damania, H. B. Shu, J. A. Duncan, J. P. Ting, NLRC3, a member of the NLR family of proteins, is a negative

regulator of innate immune signaling induced by the DNA sensor STING. *Immunity* **40**, 329–341 (2014).
16. S. Srikanth, J. S. Woo, B. Wu, Y. M. El-Sherbiny, J. Leung, K. Chupradit, L. Rice, G. J. Seo, G. Calmettes, C. Ramakrishna, E. Cantin, D. S. An, R. Sun, T. T. Wu, J. U. Jung, S. Savic, Y. Gwack, The Ca^{2+} sensor STIM1 regulates the type I interferon response by retaining the signaling adaptor STING at the endoplasmic reticulum. *Nat. Immunol.* **20**, 152–162 (2019).
17. H. Konno, K. Konno, G. N. Barber, Cyclic dinucleotides trigger ULK1 (ATG1) phosphorylation of STING to prevent sustained innate immune signaling. *Cell* **155**, 688–698 (2013).
18. Z. Li, G. Liu, L. Sun, Y. Teng, X. Guo, J. Jia, J. Sha, X. Yang, D. Chen, Q. Sun, PPM1A regulates antiviral signaling by antagonizing TBK1-mediated STING phosphorylation and aggregation. *PLOS Pathog.* **11**, e1004783 (2015).
19. T. Xia, X. M. Yi, X. Wu, J. Shang, H. B. Shu, PTPN1/2-mediated dephosphorylation of MITA/STING promotes its 20S proteasomal degradation and attenuates innate antiviral response. *Proc. Natl. Acad. Sci. U.S.A.* **116**, 20063–20069 (2019).
20. B. Zhong, L. Zhang, C. Lei, Y. Li, A. P. Mao, Y. Yang, Y. Y. Wang, X. L. Zhang, H. B. Shu, The ubiquitin ligase RNF5 regulates antiviral responses by mediating degradation of the adaptor protein MITA. *Immunity* **30**, 397–407 (2009).
21. J. Xing, A. Zhang, H. Zhang, J. Wang, X. C. Li, M. S. Zeng, Z. Zhang, TRIM29 promotes DNA virus infections by inhibiting innate immune response. *Nat. Commun.* **8**, 945 (2017).
22. Q. Li, L. Lin, Y. Tong, Y. Liu, J. Mou, X. Wang, X. Wang, Y. Gong, Y. Zhao, Y. Liu, B. Zhong, L. Dai, Y. Q. Wei, H. Zhang, H. Hu, TRIM29 negatively controls antiviral immune response through targeting STING for degradation. *Cell Discov.* **4**, 13 (2018).
23. Y. Wang, Q. Lian, B. Yang, S. Yan, H. Zhou, L. He, G. Lin, Z. Lian, Z. Jiang, B. Sun, TRIM30α is a negative-feedback regulator of the intracellular DNA and DNA virus-triggered response by targeting STING. *PLOS Pathog.* **11**, e1005012 (2015).
24. H. Sun, Q. Zhang, Y. Y. Jing, M. Zhang, H. Y. Wang, Z. Cai, T. Liuyu, Z. D. Zhang, T. C. Xiong, Y. Wu, Q. Y. Zhu, J. Yao, H. B. Shu, D. Lin, B. Zhong, USP13 negatively regulates antiviral responses by deubiquitinating STING. *Nat. Commun.* **8**, 15534 (2017).
25. Y. Chen, L. Wang, J. Jin, Y. Luan, C. Chen, Y. Li, H. Chu, X. Wang, G. Liao, Y. Yu, H. Teng, Y. Wang, W. Pan, L. Fang, L. Liao, Z. Jiang, X. Ge, B. Li, P. Wang, p38 inhibition provides anti-DNA virus immunity by regulation of USP21 phosphorylation and STING activation. *J. Exp. Med.* **214**, 991–1010 (2017).
26. T. Prabakaran, C. Bodda, C. Krapp, B. C. Zhang, M. H. Christensen, C. Sun, L. Reinert, Y. Cai, S. B. Jensen, M. K. Skouboe, J. R. Nyengaard, C. B. Thompson, R. J. Lebbink, G. C. Sen, G. van Loo, R. Nielsen, M. Komatsu, L. N. Nejsum, M. R. Jakobsen, M. Gyrd-Hansen, S. R. Paludan, Attenuation of cGAS-STING signaling is mediated by a p62/SQSTM1-dependent autophagy pathway activated by TBK1. *EMBO J.* **37**, e97858 (2018).
27. A. L. Hansen, G. J. Buchan, M. Rühl, K. Mukai, S. R. Salvatore, E. Ogawa, S. D. Andersen, M. B. Iversen, A. L. Thielke, C. Gunderstofte, M. Motwani, C. T. Møller, A. S. Jakobsen, K. A. Fitzgerald, J. Roos, R. Lin, T. J. Maier, R. Goldbach-Mansky, C. A. Miner, W. Qian, J. J. Miner, R. E. Rigby, J. Rehwinkel, M. R. Jakobsen, H. Arai, T. Taguchi, F. J. Schopfer, D. Olagnier, C. K. Holm, Nitro-fatty acids are formed in response to virus infection and are potent inhibitors of STING palmitoylation and signaling. *Proc. Natl. Acad. Sci. USA* **115**, E7768–E7775 (2018).
28. Q. Wang, X. Liu, Y. Cui, Y. Tang, W. Chen, S. Li, H. Yu, Y. Pan, C. Wang, The E3 ubiquitin ligase AMFR and INSIG1 bridge the activation of TBK1 kinase by modifying the adaptor STING. *Immunity* **41**, 919–933 (2014).
29. J. Zhang, M. M. Hu, Y. Y. Wang, H. B. Shu, TRIM32 protein modulates type I interferon induction and cellular antiviral response by targeting MITA/STING protein for K63-linked ubiquitination. *J. Biol. Chem.* **287**, 28646–28655 (2012).
30. T. Tsuchida, J. Zou, T. Saitoh, H. Kumar, T. Abe, Y. Matsuura, T. Kawai, S. Akira, The ubiquitin ligase TRIM56 regulates innate immune responses to intracellular double-stranded DNA. *Immunity* **33**, 765–776 (2010).
31. Y. Qin, M. T. Zhou, M. M. Hu, Y. H. Hu, J. Zhang, L. Guo, B. Zhong, H. B. Shu, RNF26 temporally regulates virus-triggered type I interferon induction by two distinct mechanisms. *PLOS Pathog.* **10**, e1004358 (2014).
32. G. Ni, H. Konno, G. N. Barber, Ubiquitination of STING at lysine 224 controls IRF3 activation. *Sci. Immunol.* **2**, eaah7119 (2017).
33. S. Hatakeyama, TRIM family proteins: Roles in autophagy, immunity, and carcinogenesis. *Trends Biochem. Sci.* **42**, 297–311 (2017).
34. D. Tomar, R. Singh, A. K. Singh, C. D. Pandya, R. Singh, TRIM13 regulates ER stress induced autophagy and clonogenic ability of the cells. *Biochim. Biophys. Acta* **1823**, 316–326 (2012).
35. M. Lerner, M. Corcoran, D. Cepeda, M. L. Nielsen, R. Zubarev, F. Pontén, M. Uhlén, S. Hober, D. Grandér, O. Sangfelt, The RBCC gene RFP2 (Leu5) encodes a novel transmembrane E3 ubiquitin ligase involved in ERAD. *Mol. Biol. Cell* **18**, 1670–1682 (2007).
36. C. Altier, A. Garcia-Caballero, B. Simms, H. You, L. Chen, J. Walcher, H. W. Tedford, T. Hermosilla, G. W. Zamponi, The Cavβ subunit prevents RFP2-mediated ubiquitination and proteasomal degradation of L-type channels. *Nat. Neurosci.* **14**, 173–180 (2011).
37. C. H. Ji, H. Y. Kim, A. J. Heo, S. H. Lee, M. J. Lee, S. B. Kim, G. Srinivasrao, S. R. Mun, H. Cha-Molstad, A. Ciechanover, C. Y. Choi, H. G. Lee, B. Y. Kim, Y. T. Kwon, The N-Degron pathway mediates ER-phagy. *Mol. Cell* **75**, 1058–1072.e9 (2019).
38. D. Tomar, P. Prajapati, L. Sripada, K. Singh, R. Singh, A. K. Singh, R. Singh, TRIM13 regulates caspase-8 ubiquitination, translocation to autophagosomes and activation during ER stress induced cell death. *Biochim. Biophys. Acta* **1833**, 3134–3144 (2013).
39. D. Tomar, R. Singh, TRIM13 regulates ubiquitination and turnover of NEMO to suppress TNF induced NF-κB activation. *Cell. Signal.* **26**, 2606–2613 (2014).
40. K. Narayan, L. Waggoner, S. T. Pham, G. L. Hendricks, S. N. Waggoner, J. Conlon, J. P. Wang, K. A. Fitzgerald, J. Kang, TRIM13 is a negative regulator of MDA5-mediated type I interferon production. *J. Virol.* **88**, 10748–10757 (2014).
41. B. Huang, S. H. Baek, Trim13 potentiates Toll-Like receptor 2-mediated nuclear factor κB activation via K29-linked polyubiquitination of tumor necrosis factor receptor-associated factor 6. *Mol. Pharmacol.* **91**, 307–316 (2017).
42. Z. Yu, T. Chen, X. Li, M. Yang, S. Tang, X. Zhu, Y. Gu, X. Su, M. Xia, W. Li, X. Zhang, Q. Wang, X. Cao, J. Wang, Lys29-linkage of ASK1 by Skp1–Cullin 1–Fbxo21 ubiquitin ligase complex is required for antiviral innate response. *eLife* **5**, e14087 (2016).
43. T. Saitoh, N. Fujita, T. Hayashi, K. Takahara, T. Satoh, H. Lee, K. Matsunaga, S. Kageyama, H. Omori, T. Noda, N. Yamamoto, T. Kawai, K. Ishii, O. Takeuchi, T. Yoshimori, S. Akira, Atg9a controls dsDNA-driven dynamic translocation of STING and the innate immune response. *Proc. Natl. Acad. Sci. U.S.A.* **106**, 20842–20846 (2009).
44. V. K. Gonugunta, T. Sakai, V. Pokatayev, K. Yang, J. Wu, N. Dobbs, N. Yan, Trafficking-mediated STING degradation requires sorting to acidified endolysosomes and can be targeted to enhance anti-tumor response. *Cell Rep.* **21**, 3234–3242 (2017).
45. X. Gui, H. Yang, T. Li, X. Tan, P. Shi, M. Li, F. Du, Z. J. Chen, Autophagy induction via STING trafficking is a primordial function of the cGAS pathway. *Nature* **567**, 262–266 (2019).
46. Y. Li, S. J. James, D. H. Wyllie, C. Wynne, A. Czibula, A. Bukhari, K. Pye, S. M. Bte Mustafah, R. Fajka-Boja, E. Szabo, A. Angyal, Z. Hegedus, L. Kovacs, A. V. S. Hill, C. A. Jefferies, H. L. Wilson, Z. Yongliang, E. Kiss-Toth, TMEM203 is a binding partner and regulator of STING-mediated inflammatory signaling in macrophages. *Proc. Natl. Acad. Sci. U.S.A.* **116**, 16479–16488 (2019).
47. L. Qi, B. Tsai, P. Arvan, New insights into the physiological role of endoplasmic reticulum-associated degradation. *Trends Cell Biol.* **27**, 430–440 (2017).
48. H. Chino, N. Mizushima, ER-Phagy: Quality control and turnover of endoplasmic reticulum. *Trends Cell Biol.* **30**, 384–398 (2020).
49. J. Moretti, S. Roy, D. Bozec, J. Martinez, J. R. Chapman, B. Ueberheide, D. W. Lamming, Z. J. Chen, T. Horng, G. Yeretssian, D. R. Green, J. M. Blander, STING senses microbial viability to orchestrate stress-mediated autophagy of the endoplasmic reticulum. *Cell* **171**, 809–823.e13 (2017).
50. S. Haag, M. F. Gulen, L. Reymond, A. Gibelin, L. Abrami, A. Decout, M. Heymann, F. G. van der Goot, G. Turcatti, R. Behrendt, A. Ablasser, Targeting STING with covalent small-molecule inhibitors. *Nature* **559**, 269–273 (2018).
51. M. E. McCauley, J. G. O'Rourke, A. Yáñez, J. L. Markman, R. Ho, X. Wang, S. Chen, D. Lall, M. Jin, A. K. M. G. Muhammad, S. Bell, J. Landeros, V. Valencia, M. Harms, M. Arditi, C. Jefferies, R. H. Baloh, C9orf72 in myeloid cells suppresses STING-induced inflammation. *Nature* **585**, 96–101 (2020).
52. N. Dobbs, N. Burnaevskiy, D. Chen, V. K. Gonugunta, N. M. Alto, N. Yan, STING activation by translocation from the ER is associated with infection and autoinflammatory disease. *Cell Host Microbe* **18**, 157–168 (2015).
53. J. D. Warner, R. A. Irizarry-Caro, B. G. Bennion, T. L. Ai, A. M. Smith, C. A. Miner, T. Sakai, V. K. Gonugunta, J. Wu, D. J. Platt, N. Yan, J. J. Miner, STING-associated vasculopathy develops independently of IRF3 in mice. *J. Exp. Med.* **214**, 3279–3292 (2017).
54. D. Bouis, P. Kirstetter, F. Arbogast, D. Lamon, V. Delgado, S. Jung, C. Ebel, H. Jacobs, A. M. Knapp, N. Jeremiah, A. Belot, T. Martin, Y. J. Crow, I. André-Schmutz, A. S. Korganow, F. Rieux-Laucat, P. Soulas-Sprauel, Severe combined immunodeficiency in stimulator of interferon genes (STING) V154M/wild-type mice. *J. Allergy Clin. Immunol.* **143**, 712–725.e5 (2019).
55. H. Luksch, W. A. Stinson, D. J. Platt, W. Qian, G. Kalugotla, C. A. Miner, B. G. Bennion, A. Gerbaulet, A. Rösen-Wolff, J. J. Miner, STING-associated lung disease in mice relies on T cells but not type I interferon. *J. Allergy Clin. Immunol.* **144**, 254–266.e8 (2019).
56. M. Motwani, S. Pawaria, J. Bernier, S. Moses, K. Henry, T. Fang, L. Burkly, A. Marshak-Rothstein, K. A. Fitzgerald, Hierarchy of clinical manifestations in SAVI N153S and V154M mouse models. *Proc. Natl. Acad. Sci. U.S.A.* **116**, 7941–7950 (2019).
57. B. G. Bennion, C. A. Croft, T. L. Ai, W. Qian, A. M. Menos, C. A. Miner, M. L. Frémond, J. M. Doisne, P. S. Andhey, D. J. Platt, J. K. Bando, E. R. Wang, H. Luksch, T. J. Molina, E. D. O. Roberson, M. N. Artyomov, A. Rösen-Wolff, M. Colonna, F. Rieux-Laucat, J. P. Di Santo, B. Neven, J. J. Miner, STING gain-of-function disrupts lymph node organogenesis and innate lymphoid cell development in mice. *Cell Rep.* **31**, 107771 (2020).
58. H. Siedel, A. Roers, A. Rösen-Wolff, H. Luksch, Type I interferon-independent T cell impairment in a Tmem173 N153S/WT mouse model of STING associated vasculopathy with onset in infancy (SAVI). *Clin. Immunol.* **216**, 108466 (2020).

59. S. Liu, X. Cai, J. Wu, Q. Cong, X. Chen, T. Li, F. Du, J. Ren, Y. T. Wu, N. V. Grishin, Z. J. Chen, Phosphorylation of innate immune adaptor proteins MAVS, STING, and TRIF induces IRF3 activation. *Science* **347**, aaa2630 (2015).
60. C. Zhang, G. Shang, X. Gui, X. Zhang, X. C. Bai, Z. J. Chen, Structural basis of STING binding with and phosphorylation by TBK1. *Nature* **567**, 394–398 (2019).
61. J. Wu, N. Dobbs, K. Yang, N. Yan, Interferon-independent activities of mammalian STING mediate antiviral response and tumor immune evasion. *Immunity* **53**, 115–126.e5 (2020).
62. L. H. Yamashiro, S. C. Wilson, H. M. Morrison, V. Karalis, J. J. Chung, K. J. Chen, H. S. Bateup, M. L. Szpara, A. Y. Lee, J. S. Cox, R. E. Vance, Interferon-independent STING signaling promotes resistance to HSV-1 in vivo. *Nat. Commun.* **11**, 3382 (2020).
63. B. Zhong, Y. Zhang, B. Tan, T. T. Liu, Y. Y. Wang, H. B. Shu, The E3 ubiquitin ligase RNF5 targets virus-induced signaling adaptor for ubiquitination and degradation. *J. Immunol.* **184**, 6249–6255 (2010).
64. W. W. Luo, S. Li, C. Li, Z. Q. Zheng, P. Cao, Z. Tong, H. Lian, S. Y. Wang, H. B. Shu, Y. Y. Wang, iRhom2 is essential for innate immunity to RNA virus by antagonizing ER- and mitochondria-associated degradation of VISA. *PLOS Pathog.* **13**, e1006693 (2017).
65. M. Yang, T. Chen, X. Li, Z. Yu, S. Tang, C. Wang, Y. Gu, Y. Liu, S. Xu, W. Li, X. Zhang, J. Wang, X. Cao, K33-linked polyubiquitination of Zap70 by Nrdp1 controls CD8(+) T cell activation. *Nat. Immunol.* **16**, 1253–1262 (2015).
66. Z. Yu, X. Li, M. Yang, J. Huang, Q. Fang, J. Jia, Z. Li, Y. Gu, T. Chen, X. Cao, TRIM41 is required to innate antiviral response by polyubiquitinating BCL10 and recruiting NEMO. *Signal Transduct. Target. Ther.* **6**, 90 (2021).
67. T. Chen, M. Yang, Z. Yu, S. Tang, C. Wang, X. Zhu, J. Guo, N. Li, W. Zhang, J. Hou, H. Liu, C. Han, Q. Liu, Y. Gu, C. Qian, T. Wan, L. Cui, M. Zhu, W. Zheng, X. Cao, Small GTPase RBJ mediates nuclear entrapment of MEK1/MEK2 in tumor progression. *Cancer Cell* **25**, 682–696 (2014).
68. B. C. Zhang, R. Nandakumar, L. S. Reinert, J. Huang, A. Laustsen, Z. L. Gao, C. L. Sun, S. B. Jensen, A. Troldborg, S. Assil, M. F. Berthelsen, C. Scavenius, Y. Zhang, S. J. Windross, D. Olagnier, T. Prabakaran, C. Bodda, R. Narita, Y. Cai, C. G. Zhang, H. Stenmark, C. M. Doucet, T. Noda, Z. Guo, R. Goldbach-Mansky, R. Hartmann, Z. J. Chen, J. J. Enghild, R. O. Bak, M. K. Thomsen, S. R. Paludan, STEEP mediates STING ER exit and activation of signaling. *Nat. Immunol.* **21**, 868–879 (2020).

Acknowledgments: We thank Q. Li (Chinese Academy of Medical Sciences) for providing HSV-1 (F strain). We appreciate X. Cao for the helpful suggestions and discussions. **Funding:** This work is supported by grants from the National Natural Science Foundation of China (31970892, 31770937, 31970848, 31570914, and 82001677) and the Program of Shanghai Subject Chief Scientist (18XD1405200). **Author contributions:** T.C. and J.W. designed and supervised the experiments. X.L., Z.Y., M.Y., and Q.F. did the main experiments. Q.F., J.H., and Z.L. helped with the mouse hybrid and genotyping. T.C. and X.L. analyzed data. T.C. and X.L. wrote the manuscript. **Competing interests:** The authors declare that they have no competing interests. **Data and materials availability:** All data needed to evaluate the conclusions in the paper are present in the paper and/or the Supplementary Materials.

Submitted 11 February 2021
Accepted 30 November 2021
Published 26 January 2022
10.1126/sciadv.abh0496